Compound flooding from storm surges, rivers, and groundwater - Hydrodynamic modelling in a coastal catchment

IK Seidenfaden[1*], MR Skjerbæk[1], HJ Henriksen[1], KK Kjeldsen[1], TO Sonnenborg[1]

[1]Geological Survey of Denmark and Greenland, GEUS, Øster Voldgade 10, 1350 Copenhagen K, Denmark

Corresponding author: Ida Karlsson Seidenfaden (ika@geus.dk)

Key Points:

- The largest river stage extremes were dominated by compound effects from two or more drivers (precipitation, groundwater and sea level)
- High groundwater tables were routinely registered for flooding events with the largest spatial extent of water on terrain

Abstract

Coastal zones are particularly vulnerable to flooding. Several climatic and state variables may drive the occurrence of such events, e.g., storm surges, sea level rise, heavy rainfall, and high river and groundwater levels. The co-occurrence of such events, i.e. compound or cascading effects, has been shown to escalate flooding impacts and extent, but the contribution of groundwater is routinely overlooked. Here, we apply an integrated hydrological/hydrodynamic/groundwater model to investigate underlying causes and compound effects in a Danish Wadden sea catchment. Two models were developed: a long-term model and an overbank-spilling model. The long-term model was calibrated and used to simulate 30-year periods. Extreme value analyses were carried out for sea levels, precipitation, simulated river water stages, and groundwater levels. The co-occurrence of extremes was used to identify compound effects on high river-stage incidents (as a flood proxy). The overbank-spilling model was then used for simulating flooding for a subset of the largest river stage events identified from the long-term model. The analysis showed that the river-stage events were closely correlated to the sea level extremes, but that the largest river-stage events were almost exclusively compounded by precipitation or groundwater, or both. High groundwater tables seem to correlate to the flooding events with the largest spatial extent, as well as prolonged extreme events where either precipitation or sea level were elevated during long periods. Thus, this study shows that there is a general need to acknowledge the potential effect of groundwater levels on the resulting flooding on terrain in coastal zones.

Keywords: flooding, compounding, sea level, river stage, hydrodynamical modelling, groundwater modelling, flood plain, marshland

1 Introduction

Low-lying coastal areas are especially exposed to flood risks. According to McGranahan et al. (2007), approximately 2% of the earth's land surface can be classified as a Low Elevation Coastal Zone (LECZ), defined as all coastal areas with an elevation below 10 meters above mean sea level. At the same time, the LECZ is inhabited by approximately 11% of the world's population (Magnan et al., 2022), with significantly higher population densities than in non-coastal zones (Neumann et al., 2015). This makes it particularly vulnerable to flooding. With a share of 26% of the total land area located in the LECZ, Denmark is among the 10 countries with the highest share globally (McGranahan et al., 2007).

Floods in coastal areas are typically caused by storm surges, high tides, or heavy rainfall, causing river water levels in low-lying delta areas to rise above the banks (Santiago-Collazo et al., 2019). Often, these events happen simultaneously or in close temporal succession, as the driver is low atmospheric pressure events, often leading to strong winds and heavy rainfall at the same time (Bevacqua et al., 2019; Dykstra and Dzwonkowski, 2021; Hendry et al., 2019). In the Special Report of the Intergovernmental Panel on Climate Change (IPCC) on Managing the Risks of Extreme Events and Disasters to Advance Climate Change Adaptation (SREX) (Seneviratne et al., 2012), this co-occurrence of events is termed compound events. Several studies have investigated compound events governed by high sea levels caused by storm surges and precipitation (Lian et al., 2013; Qiang et al., 2021; Wahl et al., 2015). Zellou and Rahali (2019) investigated the statistical significance of the concurrence of storm surges and heavy precipitation events in Bouregreg River (Morocco) and found that the largest effect may be from heavy rainfall events. Especially west-facing European coasts have been found to be prone to compound effects (Heinrich et al., 2023).

Existing infrastructure such as dams and dikes in combination with river locks/barriers is another important factor when analysing coastal floods (Kew et al., 2013). However, few studies include the effect of protective infrastructure such as dikes and river locks (Tang and Gallien, 2023). If such structures exist, it is especially important to investigate the effects of compound events, since the simultaneous occurrence of a storm surge, causing water levels at the outside of the barrier to rise, and heavy precipitation, causing water levels at the inside of the barrier to rise, leading to the problem of getting flooded by either seawater (when the barrier is left open) or by river water when the barrier is closed because of elevated sea levels (Van den Brink, 2005).

The groundwater levels, and thus subsurface storage of the basin, can also play an important role in the response of the hydrological system to heavy rainfall and/or closed drainage structures to the sea (Tang & Gallien, 2023). However, this mechanism is not yet well comprehended and understudied (Rahimi et al., 2020). Neri-Flores et al. (2019) carried out a study in a city in the Gulf of Mexico where the effect of groundwater and river flooding was monitored. The study found that groundwater flooding was frequent on the floodplain. Peña et al. (2022) simulated three flooding events with a coupled FLO-2D and MODFLOW model in Florida, USA. The events had high rainfall, water table and normal tide conditions to investigate the groundwater contribution. They found that groundwater flooding influenced the flooding from the river system, and is particularly important in karstic areas, where groundwater heads are likely to react fast to high precipitation events. To our knowledge, no studies yet exist that investigate the influence of shallow groundwater levels on the occurrence and extent of fluvial flooding in combination with elevated sea levels and extreme precipitation.

When evaluating and monitoring underlying mechanisms and causing drivers of coastal flooding, several methods have been described in the literature. They can be grouped into three main approaches: empirical/statistical methods (e.g., satellite imaging), simplified methods such as distributing water on a DEM e.g., Dutta (2011); Poulter and Halpin (2008); Tang and Gallien (2023); Teng et al. (2017)), and 1D, 2D or 3D hydrodynamic numerical models e.g., Anselmo et al. (1996). Numerical models are, however, necessary for studies where the system dynamics and responses are investigated and where investigations of groundwater levels are to be carried out. In the present study, a modelling system with an integrated framework and a coupled groundwater component is essential.

In the studies presented above a "forward approach" is applied, where extreme events are identified from inspection of the forces driving the resulting flooding (impact). In contrast, we apply a "reverse" or "bottom-up" approach, where the starting point for the different analyses are river water stages as a result of various driving forces. An integrated hydrologic/hydrodynamic model is executed for a 30-year period and the resulting most extreme river water levels are selected (the possibility for flooding on the surface is highest, i.e., impacts) as a point of departure for our compound event analysis using enhanced flood process description in hydrodynamic model. Periods containing events that are most prone to flood are analysed and the co-occurrence of extremes in the three driving forces (sea level, precipitation, and groundwater levels) are identified. The analysis is carried out for a study area at the Danish Wadden Sea with a history of devastating floods caused by large storm events, that have motivated the construction of several dikes with large river locks at the river outlet. The objectives of this study are the following:

(1) To set up and calibrate a hydraulic river flow model to make it possible to reproduce the effect of river locks and tidal variations on river water levels.
(2) To build a version of the hydraulic river flow model that makes it possible to simulate flooding for selected events.

(3) To carry out extreme value analyses for river water stages and corresponding external-catchment forcing (i.e., sea levels and precipitation) as well as the hydrological state of the catchment (i.e., groundwater levels) to identify compound effects on the occurrence of flooding.
(4) To simulate selected flood events with different (combinations of) drivers, based on the analysis from (3).

2 Study site

The catchment of Ribe River, located in western Denmark, was selected as a study area. The Ribe catchment has an area of 981 km^2 and is drained by the Ribe River that flows from east to west where it discharges into the Wadden sea tidal area connected to the North Sea. The terrain elevation is highest to the east and slopes towards the west coast where an outwash plain and marsh plains of low relief form the costal line. However, low relief less than 5 meters above sea level is found all the way up to the city of Ribe (black line indicated in Figure 1 – right), which is the main focus area of the study.

The climate is moderate maritime, and the catchment mean annual precipitation is 960 mm/y (in 2010-2020) with average temperatures of 9.0 degrees Celsius (in 2010-2020). The land use in the catchment is dominated by agricultural lands, with winter crops and spring crops being the dominating crop types. 11% of the catchment is covered by forest and 7.1% consists of urban or suburban areas. Sandy soils (52%) are predominant, scattered with moraine deposits, mainly consisting of clayey till (33%), and freshwater deposits along streams and lakes (11%). The geology is governed by sandy and gravelly meltwater deposits from the Pleistocene glaciations.

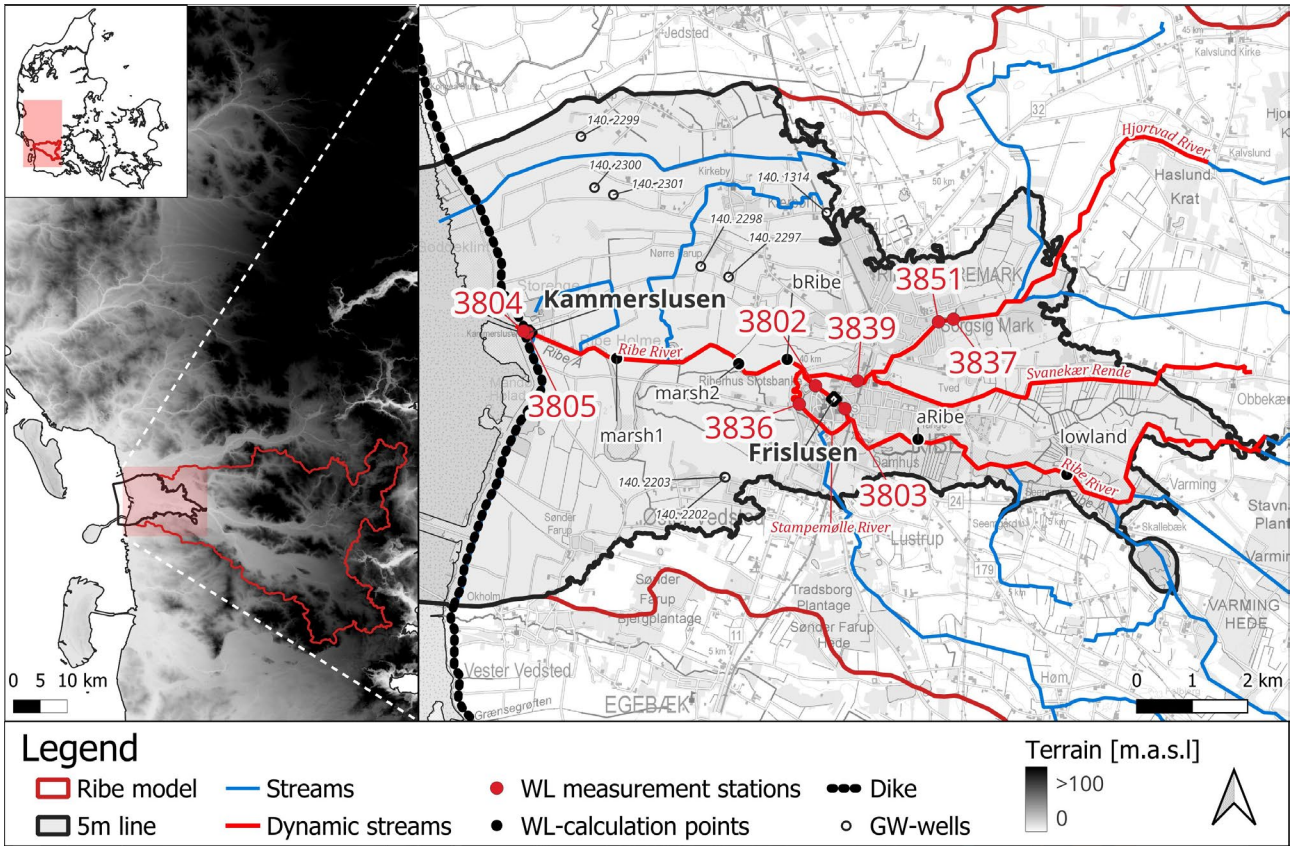

Figure 1: Overview of the Ribe catchment with an indication of stream discharge and water level stations. The area outlined by the black line indicates the focus area (below 5 meters above sea level). Also indicated are the main canals ("Dynamic streams"), where the river modelling is changed to hydraulic.

Several historical extreme flooding events have been observed in the catchment. A sea level of six meters above normal was registered in 1634. Since no dikes existed at this time, the entire city of Ribe was flooded with a water level of 1.70 meters inside the city's cathedral and many lives were lost (TheDanishNatureAgency, 2023). Other storm events with high sea levels and significant losses of lives and destruction of property are known for the years 1362 and 1825 (Historiskatlas, 2023; TheDanishNatureAgency, 2023). Also in 1911, 1928, 1936, 1968, 1976, 1981, 1990, and 1999 sea levels rose significantly above normal, with the largest of these events being in 1999, where the sea level gauge at the outlet of the Ribe River collapsed at 5.12 meters above normal, but a maximum sea level of 5.50 meters was estimated (TheDanishNatureAgency, 2023).

Since 1914 the dike along the coast and an automatic sluice (Kammerslusen) at the outlet of the Ribe River have protected the city from flooding from seawater (Historiskatlas, 2023; Piontkowitz et al., 2011). The sluice is closed when the water level in the sea is above the water level in the Ribe River, and open when it is below. The tidal difference in the sea outside the dike is around two meters. In addition to Kammerslusen, there is a smaller gate further upstream in Ribe River, located at the city centre of Ribe (Frislusen). This gate is used to control the water level in the river and wetland upstream of the city, and it is closed as soon as the water level just upstream of the gate falls below a certain level, varying by season. However, high sea levels still pose a problem, since it results in prolonged periods where the gate closed resulting in accumulation of water drained from the catchment, thus elevating the risk of flooding from backwater.

147 2.1 Observational data

148 The climatological data used as input for this study consists of the Denmark's Meteorological
149 Institute (DMI, 2022) dataset of 10x10 km gridded precipitation dataset, and 20x20 km temperature
150 and potential evapotranspiration datasets (Scharling and Kern-Hansen, 2012), calculated using the
151 Makkink formula (Makkink, 1957).

152 Sea level data was obtained from Climate Atlas run by the Coast Directorate of Denmark.
153 Tide station 38.04 is located at the seaside of the sluice (Fig. 1). Sea water level has been recorded
154 every 5 minutes in the period of 1990-2023. However, the sea level data is not complete and the time
155 series from nearby stations at Højer (9.6 km) and Mandø (40.6 km) are therefore used for gap filling
156 of missing records (see sec. 3.1).

157 There are three types of hydrological data in the catchment utilized in this study. For the river,
158 there are 5 gauging stations that measure stream flow discharge, while there are 8 stations with
159 measurements of water stage within the low relief area of interest. The groundwater monitoring
160 dataset consists of 26 hydraulic head wells with time series measurements.

161 Synthetic Aperture Radar (SAR) satellite images from the European Space Agency's (ESA)
162 Sentinel-1 mission are used for validating the simulated extent of water on the surface during flooding
163 events. These are obtained from ESA's Copernicus Open Access Hub (ESA, 2023a). The mission
164 consists of two satellites, the first of which was launched in April 2014 and the second one in April
165 2016. The temporal resolution of images from each satellite is approximately 12 days, i.e.,
166 approximately 6 days after April 2016, where two satellites are operating, while the spatial resolution
167 is 10-40 m, depending on the acquisition mode. The advantage of using SAR-data is that it is acquired
168 at wavelengths, which depend neither on daylight nor the absence of clouds.

169

170 **Table 1 Overview of data and sources used in the study.**

Data type	*Type*	*Spatial resolution*	*Temporal resolution*	*Reference*
Gridded	Precipitation	10 km	Daily	Scharling and Kern-Hansen (2012)
	Temperature	20 km	Daily	Scharling and Kern-Hansen (2012)
	Potential evapotranspiration	20 km	Daily	Scharling and Kern-Hansen (2012)
	Land use	100m	Constant	Levin et al. (2012)
	Crops	Field	Constant	Ministery of food
	Soils	10m	Constant	DCA (2014)
	Satellite flood data	10-40 m	Approx. 6 days	ESA (2023)
Point	Sea level	3 stations	Hourly	DMI (2022)
	Stream discharge	5 stations	Daily	Odaforalle (2021)
	Stream water level	8 stations	Hourly	Odaforalle (2021)
	Groundwater heads	26 wells	Daily	GEUS (2014)

171

3 Methods

3.1 Data processing and quality assurance

Sea level data is available for three stations: the primary station at the outside of Kammerslusen at the outlet of the Ribe River to the sea, and two secondary stations (Table 2). Data for the latter two is used to fill gaps in the time series for Kammerslusen. Some data were missing at all three stations, and there were several timesteps with unlikely and erroneous data (typically the same value for several hours or days in a row). The latter was identified by plotting the data, manually scrutinizing it month by month and deleting the problematic data.

Table 2: Sea level data.

Station name	*Station number*	*Start date*	*End date*	*% missing*	*R^2 for correlation with 38.04*
Kammerslusen	38.04 (6701)	01-01-1991	31-12-2020	1.98	-
Højer	6501	01-01-1991	31-12-2010	0.50	0.95
Mandø	7101	02-11-2000	31-12-2020	3.34	0.94

After removing all erroneous data for all three sea level stations, the gaps in the time series for Kammerslusen are filled by using correlation equations obtained from scatterplots for data from Højer/Kammerslusen and Mandø/Kammerslusen respectively. The former had a slightly higher R^2 value and is thus prioritized in the overlapping period between 2000-2010. After gap filling, an almost complete sea level time series for the period 1991-2020 is obtained for station 38.04; only 0.36% of data are missing, compared to 1.98% before (Table 2).

In addition to that, data for the sea level Kammerslusen is quality-checked by comparing it to water level data for the inner station at Kammerslusen (38.05): The gate is closed when the water level in the sea is above the water level in the river; thus, the minimum values for the two stations must be the same (i.e., when the gate is open). This was true most of the time; however, for the whole of 2008, the minimum water level at the inner station at Kammerslusen was above the minimum water level at the outer station. When comparing with the sea level data from the two other sea level stations, it became obvious that it was data for the inner station at Kammerslusen which was erroneous.

For the satellite imagery, images were available for two flooding events in the calibration period – one for January 2015 (12th of January 2015; 5:48 am), and one for February 2020 (21st of February 2020, 5:48 am). The raw satellite images were processed by using ESA's Sentinel Application Platform (SNAP) software (ESA, 2023b); here the images are binarized to separate water pixels from non-water pixels.

3.2 The hydrological models

For this study, the impact model is a subset of the newest version of the National Hydrological Model of Denmark (Henriksen et al., 2020; HIP, 2022). It is modified and developed further, to be able to model river structures, tidal impacts on river water levels, and flooding (section 3.2.1). Due to the computational burden of flooding calculations, simulation of flooding is only done for selected events, furthermore, different convergence parameters are needed for model with and without the

206 flooding component, resulting in two versions of the model (*The Ribe model* – long term, section
207 3.2.2, and *The Ribe flood model* – event simulations, section 3.2.3).

208 ### 3.2.1 The baseline hydrological model (HIP4Plus)

209 The baseline hydrological model is a subset (sub-model) of the newest version of the National
210 Hydrological Model of Denmark, called the HIP4Plus model (Henriksen et al., 2020; Henriksen et
211 al., 2023; HIP, 2022). The HIP4Plus model is built in the integrated grid-based MIKE SHE modelling
212 framework (Abbott et al., 1986; DHI, 2019), and is based on the National Hydrological Model, which
213 has been developed and updated continuously during the last 20 years (Henriksen et al., 2003;
214 Højberg et al., 2013). The MIKE SHE modelling tool contains several solution engines for the
215 different flow compartments, and the HIP4Plus model uses the 2-layer evapotranspiration module,
216 degree day snow, 1D unsaturated zone (2-layer), 2D overland flow, a 2D river flow routing in
217 MikeHydro, and a 3D finite-difference groundwater flow solution in a 100x100 m grid. The complete
218 HIP4Plus model (Schneider et al., 2021) covers the entire of Denmark and is comprised of seven
219 domain models (DK1-7). The model is calibrated using an extensive set of streamflow discharge
220 observations (>300) and hydraulic head measurements (>25,000). The HIP4Plus model is calibrated
221 using the PEST calibration tool, with a multiple objective function consisting of Kling-Gupta
222 efficiency on stream discharge, annual and summer water balance and root mean square error on
223 hydraulic heads, as well as irrigation amounts. More information on the calibration setup of the
224 HIP4Plus model can be found in Schneider et al. (2021) and (Henriksen et al., 2020).

225 The Ribe catchment is located in domain DK4. The sub-model covers 981 km^2 and contains
226 121 stream discharge stations and 205 hydraulic head observations. The model is cut out from the
227 larger HIP4Plus model and covers the entire topographical catchment drained by the Ribe river
228 network. No flow boundaries are set along the edges of the catchment to the east, north and south,
229 while the North Sea constitutes the boundary to the west, as the area constitutes a complete water
230 catchment.

231 ### 3.2.2 The Ribe model

232 Due to the scale of the national HIP4Plus model, the conceptual setup of the river system in
233 Ribe is simple (routing) and local water features are not originally incorporated into the model.
234 Therefore, numerous adjustments are necessary to obtain a model able to simulate local dynamics
235 and accurate river water levels. These updates are performed in the sub-model setup to create the Ribe
236 model. The most important change compared to the baseline model is moving from river flow routing
237 to hydraulic modelling of river flow in the main canals (Figure 1); this enables the model to move
238 from simulating not only realistic streamflow quantities, to also simulating realistic dynamic water
239 stages in the river. This change also means that the river stage can respond correctly to tidal changes
240 at the outlet.

241 The simulation of the water stage in the river is dependent on correct cross-section data of the
242 river structure, therefore an extensive update with new data and quality check of the cross-sectional
243 data has been performed throughout the river reach. These include:

244 - Incorporation of the main river sluice (Kammerslusen) where the river discharges to the sea
245 - Change of boundary condition in the Ribe River to time-varying sea level at the outside of
246 Kammerslusen
247 - Incorporation of river sluice (Frislusen) in Ribe

- Incorporation of water level data for calibration/verification (6 stations, Figure 1)

Because of the rigorous and thorough calibration already performed during the setup of the baseline HIP4Plus model, and because no changes have been made in the hydrogeological setup of the model, the calibration of the Ribe model concentrates on the simulated river stages compared to the measured. However, a comparison of the stream discharge and hydraulic head performance for the Ribe and the baseline model is reported (Figure 2), to ensure that there was no loss of performance when modifying the river setup. The river network is calibrated for the period of 2008-2020, by manually adjusting the Manning number in the different river sections. The seasonal variation of the Manning number is described by a sinus curve representing the variation of vegetation in the stream; the Manning number adjustment moves the curve up or down.

3.2.3 The Ribe flood model

Flood modelling is performed using the overbank spilling method, where river water is spilled on the surface as soon as the water level in a stream exceeds one or both bank levels. Here, the riverbanks are treated as broad crested weirs, and the spilling is calculated by the standard broad crested weir formula (DHI, 2020). This calculation requires very small timesteps and thus increases the computational burden of the simulations dramatically; it is therefore not possible to run the model with flooding for multiple years. Furthermore, adjustments in solvers, timesteps, and numerical iteration parameters are often needed to make the flood modelling converge. To overcome this obstacle, a tuned flood model is developed that only runs in the months surrounding selected events, identified based on high river stages in the Ribe model (section 3.3).

The Ribe flood model is not calibrated further, but to investigate the validity of the flood modelling results, flood modelling is simulated for two historical flooding events: The 12th of January 2015 and the 22-23rd of February 2020. The spatial extent of flooding is evaluated by using satellite images from ESA's Sentinel-1 Synthetic Aperture Radar (SAR)-data for the two events (see section 4.1) as well as comparing simulated river water levels to observations.

3.3 Flooding and river stage event identification

The impact event of interest in this study is the risk of flooding on the land surface. As mentioned in sec. 3.2.2 it is not possible to model the impact events (flooding on land) for the complete 30-year period, and thus the impact events cannot be assessed directly from the Ribe model results. However, historical local knowledge has shown that after the construction of the dike in 1914, flooding events were mainly a result of high river stage (REF) and overbank spilling. It was therefore chosen to identify potential flood events by the river stage events.

The long-term Ribe model is, therefore, used to identify and analyse occurrences of high river water stage during the 30 years. An extreme analysis is run for the water stage at 8 points equally distributed from the coast to the lowland area upstream of Ribe city (Figure 1), to ensure that the river extremes occurring on both ends of the reaches (up- and downstream) are represented. The return levels for a 2 yr., 5 yr., 10 yr., 50 yr., and 100 yr. event (T2, T5, T10, T50 and T100) are calculated using the EVA tool (DHI, 2024), as well as the 90-, 95-, and 99-percentile of the river stage for each point. The EVA tool uses the Annual Maximum Series (AMS) method for the extraction of the extremes. The extreme values time series is then fitted using the Generalised Extreme Value distribution using the estimation method of L-moment.

To identify unique river stage events across multiple locations a systematic identification method was developed. First, the water level is compared to a threshold over which there is a flood possibility, a flood identification limit, at every time step (1 hour) in each of the selected eight locations on the river network. For each location, the exceedances are first pooled when they are occurring successively into a location-specific-episode with a start and end time. These location-specific episodes are then merged in space so that overlapping location-specific episodes occurring simultaneously in multiple locations are merged, thus creating spatially spanning river events with start and end time, as well as (number of) locations where it occurs. The overlap does not have to be precise but rather any location-specific episode that at some time during its period overlaps with another location-specific event is merged, accounting for delays in the system. Thus, a river event can for instance cover a location-specific-episode at location 1 from timestep 0-5, and location-specific-episodes at locations 2 and 3 from timestep 4-10, resulting in a total event time of 0-10. The resulting river event is therefore bounded by a start (first overshoot hour) and end (last hour of overshoot), a peak water level (defined by date and location) as well as a number of locations on the river that are affected.

River events may be discontinued by shorter time spans where the water stage is below the flood identification limit and these separated events may thus be assumed to be highly correlated. Therefore, a correlation threshold is defined, given as a certain allowed span of pause time under which the events are merged. Thus, the result is a list of uniquely separated river stage events occurring at one or more locations on the river network. To avoid small and local events, events can also be filtered out based on how many locations they occur. Information about the final river stage events is then logged, this information includes timing, duration, maximum water stage exceedance, maximum event type (T2, T5 …) reached (as a measure of severity) and the average exceedance i.e., mean above flood identification limit (as a measure of intensity).

3.4 Compound analysis

For every river stage event, identified in 3.3, the sea level, precipitation and groundwater are then evaluated and registered. As for the river water stage, the driving conditions are also evaluated using the extreme event analysis tool EVA (DHI, 2024), identifying return periods of T2, T5, T10, T50 and T100, and by the 90-, 95- and 99-percentile following the same procedure as for the water level time series. According to the definition of compound events, none of the contributing drivers have to be extreme by themselves, to lead to an extreme impact (such as a flood). This is the reason for including Q90, Q95 and Q99 in the analysis of driving variables. Leonard et al. (2014) refine the definition from the SREX to the following "*A compound event is an extreme impact that depends on multiple statistically dependent variables or events.*", thus the term can be used to highlight the resulting impact. This means that a compound event caused by multiple variables is only classified as extreme if its impact is extreme, on for example infrastructure and/or human health and life.

Zscheischler et al. (2020), suggest a typology for compound events, providing a coherent framework for the analysis of such events into four typologies: *preconditioned*, *multivariate*, *temporally compounding*, or *spatially compounding*, that can be used in combination to classify events. The preconditioned typology refers to compound events that occur only because of an already-present condition, this in combination with a new event leads to an extreme impact. The multivariate topology covers all compound events that are driven by more than one driver in the same area that may or may not be related. Temporally compounding covers compound events that are caused by several events occurring one after the other over time, thus in the end resulting in extreme impacts.

Spatially compound covers events that occur in different locations at the same time, but together lead to an extreme impact. These types were also illustrated with examples by Bevacqua et al. (2021).

With regards to flooding in low-lying coastal areas, the compounding events are often multivariate (Zscheischler et al., 2020) where the main forcing/drivers are the sea level, river flow stage, and precipitation, as well as several wind characteristics (often driving elevated sea level situations). However, the preconditioning of the area can play an important role in the occurrence of flooding; as a high degree of soil saturation and terrain near groundwater levels, e.g., as a result of extended periods of continuous precipitation, will make areas more vulnerable to flooding during even minor storm surge or precipitation events, which otherwise could have been accommodated within the hydrological system. Thus, the hydrological system can respond in a non-linear way to the outside catchment forcing, potentially buffering or accelerating the flooding. In this study, the preconditioned events are therefore examined by investigating the groundwater system state. The identified river stage events will, therefore, be correlated to forcing (precipitation and sea level) and preconditioning (groundwater) in an analysis of main drivers and compound types and effects (see sec. 3.4). Based on these results selected river stage events will be modelled with the Ribe flood model to create the impact event (flooding on land) and analyse the actual resulting flooding from different historical situations.

3.4.1 Forcing (precipitation and sea level)

Precipitation is given in daily resolution and is investigated as a catchment average. The occurrence of maximum precipitation and maximum river stage peak may not be exactly correlated in time, meaning that a high precipitation event may manifest in the river system with delays due to response times of the system, depending on soils, geology, and catchment size. Furthermore, the timing of the maximum river stage is also associated with some uncertainty. To account for this, the Spearman Rank Correlation is used to find the best correlation between precipitation conditions and river events, using different buffer windows (all combinations of +1 day to +8 days and -1 day to -8 days). The correlation between precipitation and river events is used to determine an appropriate buffer range of days before ($Pbuffer_{before}$) and days after ($Pbuffer_{after}$) the maximum river stage peak when looking for correlated precipitation conditions. The sea level data is given every hour and the extreme event analysis is conducted on this resolution. Even though maximum sea level and maximum river stage peak could be assumed to be well correlated in time, they may diverge after the river lock closes and the two water stages on each side may evolve with different speeds and strength. Therefore, the sea level correlation to the river events is also investigated using the Spearman Rank Correlation for different buffer windows (all combinations of half day-windows of +0.5 day to +8 days and -0.5 day to -8 days), determining the appropriate buffer range of hours before ($SLbuffer_{before}$) and days after ($SLbuffer_{after}$). The identification of compounded forcing variable, thus, is done in these 3 steps for every river event:

1. Recognition of the river maximum date and time, (Rmaxdate), from the analysis described in 3.3.
2. Identification of most extreme daily precipitation status in the time window of [Rmaxdate-$Pbuffer_{before}$:Rmaxdate+ $Pbuffer_{after}$], possible outcomes are noevent, Q90, Q95, Q99, T2, T5, T10, T20, T50 or T100.
3. Identification of most extreme hourly sea level status in the time window of [Rmaxdate-$SLbuffer_{before}$:Rmaxdate+ $SLbuffer_{after}$], possible outcomes are noevent, Q90, Q95, Q99, T2, T5, T10, T20, T50 or T100.

Apart from being related to daily/hourly forcing events, critical compound events in the river may also be related to prolonged periods of elevated precipitation or sea level, that isolated may not in themselves be extreme but may lead to extreme river conditions due to their duration. To investigate this the precipitation and sea level records are both investigated for longer temporal extremes. The long-term extremes are identified by averaging the precipitation and sea level time series with running means and then calculating the percentile to determine if the long-term mean is uncommonly high, in these three steps:

1. Recognition of the river maximum date and time, (Rmaxdate), from the analysis described in 3.3.
2. Calculating the percentile for a backward rolling mean precipitation time series on Rmaxdate, possible outcomes are between Q0-Q100. Rolling means are calculated for intervals of 7, 14, 21 and 28 days.
3. Calculating the percentile for a backward rolling mean sea level time series on Rmaxdate, possible outcomes are between Q0-Q100. Rolling means are calculated for intervals of 7, 14, 21 and 28 days.

3.4.2 Preconditioning (groundwater)

For the groundwater, it is expected that the response time is substantially slower than for the other parts of the system. Furthermore, like the groundwater will affect the river stage, groundwater levels can also reversely be affected by a high river stage. As the purpose of the groundwater analysis is to investigate the preconditioning it was chosen to look at longer time scales. The groundwater extremes are, therefore, calculated for a period of 14 days and matched with the river maximum stage. As the groundwater is a spatially distributed variable, the extreme analysis becomes somewhat more challenging. Here we have chosen to limit the investigation area to within the 5-meter elevation line (Figure 1). The extreme analysis can then be done for each grid of the area for the 90-, 95- and 99-percentile and the return periods of T2, T5, T10, T50 and T100. To facilitate the compound analysis, a mean groundwater level is calculated for the area, and an extreme analysis is also performed for this mean time series. This time series together with the percentage of the grid above T2 for the timesteps will be used for correlation to the river events in the compound analysis.

4 Results

4.1 Calibration and performance of the hydrological models

As mentioned above, only the river setup is calibrated by adjustment of the Manning number for the period 2008-2020 in the Ribe model. In the baseline model setup, the Manning number was 25 $m^{1/3}/s$ for all branches, with an average absolute mean error of 0.94 m for the river water levels. Manning number values of 15 and 35 $m^{1/3}/s$ were tested for all dynamic branches, while manually comparing simulated water levels to observed ones. This resulted in optimal Manning numbers of 15 $m^{1/3}/s$ for Hjortvad River as well as the lower part of Ribe River, and 25 $m^{1/3}/s$ for all remaining branches. The calibration of the Manning number led to a substantial reduction of the average mean absolute error (MAE) for river water levels to 0.21 m (Figure 2). The largest reductions are seen for the three stations in the Ribe River, with a reduction of the MAE from 2.92 m to 0.19 m for the station at Kammerslusen (3805), from 1.05 m to 0.15 m for the station downstream Frislusen (3802) and from 0.56 to 0.08 m for the station upstream Frislusen (3803). For the RMS the pattern is similar, with reductions from 2.94 to 0.25 m, 1.09 to 0.18 m, and 0.61 to 0.10 m for the three stations,

respectively. Thus, the further upstream, the smaller the improvement of model performance, i.e., the smaller the effect of the introduction of the hydraulic method for flow modelling. This is not surprising, since the tidal effect is the largest the closer to the river outlet, and since it is not simulated in the HIP4Plus model, the differences will be largest at places with large tidal effects. This also implies that the effect is much smaller for the three remaining stations (3836, 3839 and 3837).

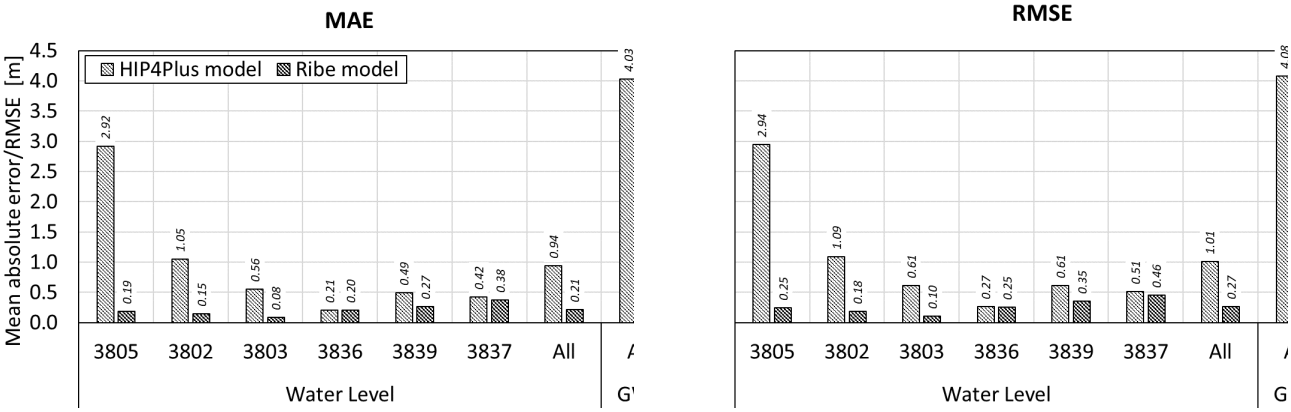

Figure 2: Model performance for HIP4Plus for selected water level stations and all groundwater wells in the model area (calibration period 2008-2020).

For the 16 groundwater head time series in the model area, the average for both MAE and RMS is just above 4 m (Figure 2; see individual well performance information in S-Table 2) both for the HIP4Plus model and the Ribe model. The same is the case for discharge (S-Table 1). Thus, there is no reduction in performance for these two variables with the introduction of a hydrodynamic simulation routine in the main river.

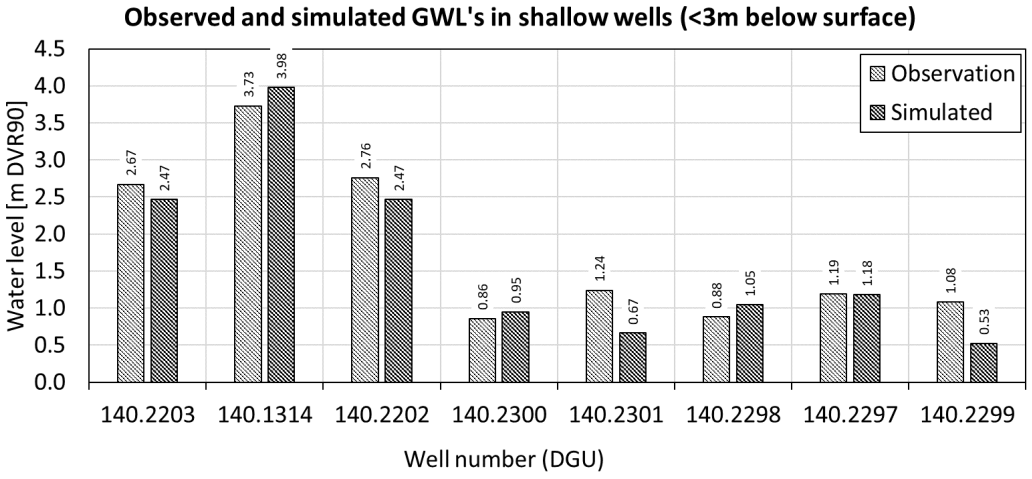

Figure 3: Observed and simulated groundwater levels in shallow wells (<3 m below surface) in the focus area.

The Ribe flood model is also evaluated for two historical flooding events: The 12th of January 2015 and 22-23rd of February 2020. Temporal performance is tested by comparing simulated to observed water stages at the three stations in Ribe river (Figure 4), while the spatial performance is evaluated by using satellite flood images (Figure 5). For both flooding events, the dynamics in water levels are improved considerably by incorporating our flood modelling scheme, especially in periods

with high water stages, such as between January 9-11th 2015 and February 9-12th 2020; this being especially the case for the two stations downstream Frislusen (3805 and 3802; Figure 4). Summary statistics MAE and RMS are equally slightly improved at all three stations (Figure 4).

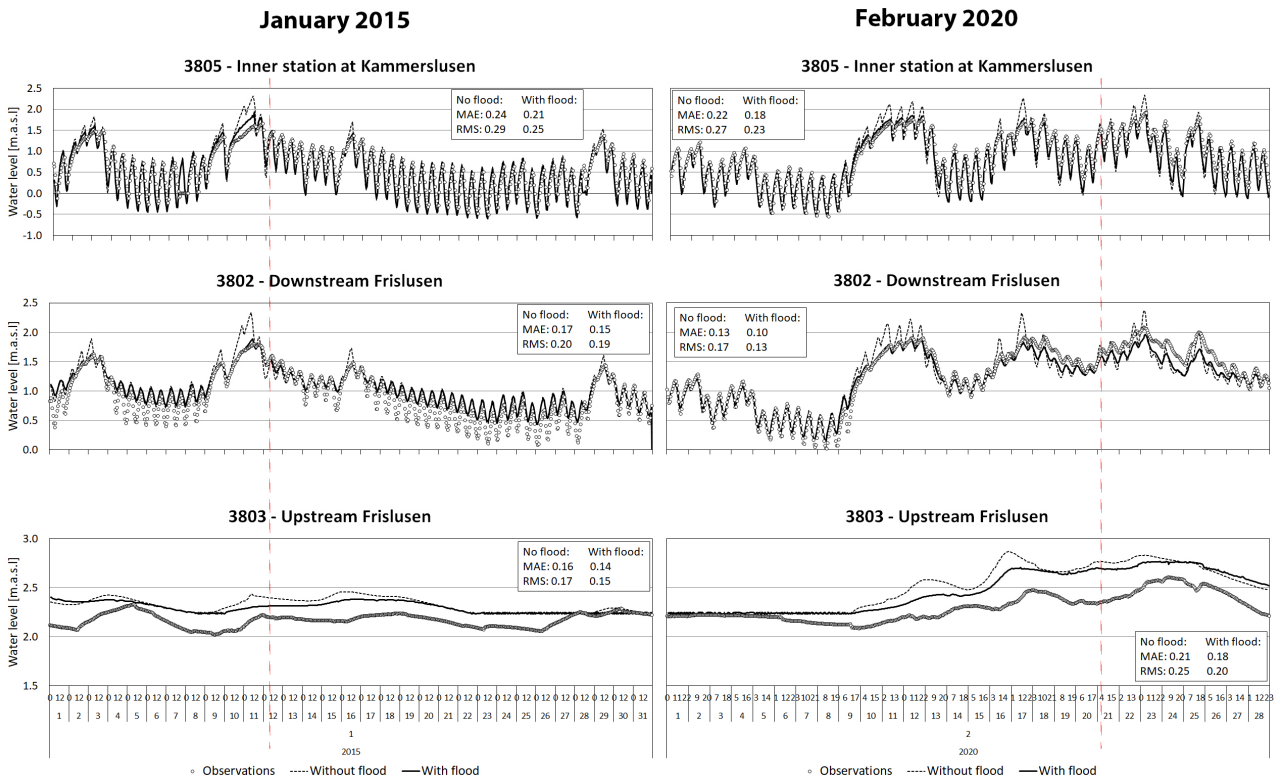

Figure 4: Water stage performance of the calibrated Ribe Flood model for three water level stations during the flooding events of 12/01/2015 (left) and 21/02-2020 (right). The dotted black line in the graphs shows the resulting water levels when running the model without flooding. The dotted red lines show the temporal location of the water-on-surface maps.

Figure 5 shows the extent of water on surface resulting from the analysis of Sentinel-1 satellite images as well as the Ribe flood model; areas with observed water on surface are shown in red, while simulated areas are shown in blue shading. Overall, the extent of water on surface is simulated fairly well during both flooding events, with the locations of both observed and simulated areas overlapping widely. However, an overestimation of the model can be seen for both events southwest of the Ribe river, as well as north of the wetland area to the east of the city of Ribe; the latter being mostly the case during the 2015-event. In contrary, in the marsh area north of the Ribe river, the model slightly underestimates the extent of water on surface for both events. Nonetheless, considering the uncertainties connected to both modelling and the analysis of satellite images (selection of threshold values, effects of vegetation on detection of water on surface etc.), we find overall good agreement between the observations and simulated water extent and regard our model performance as rather good.

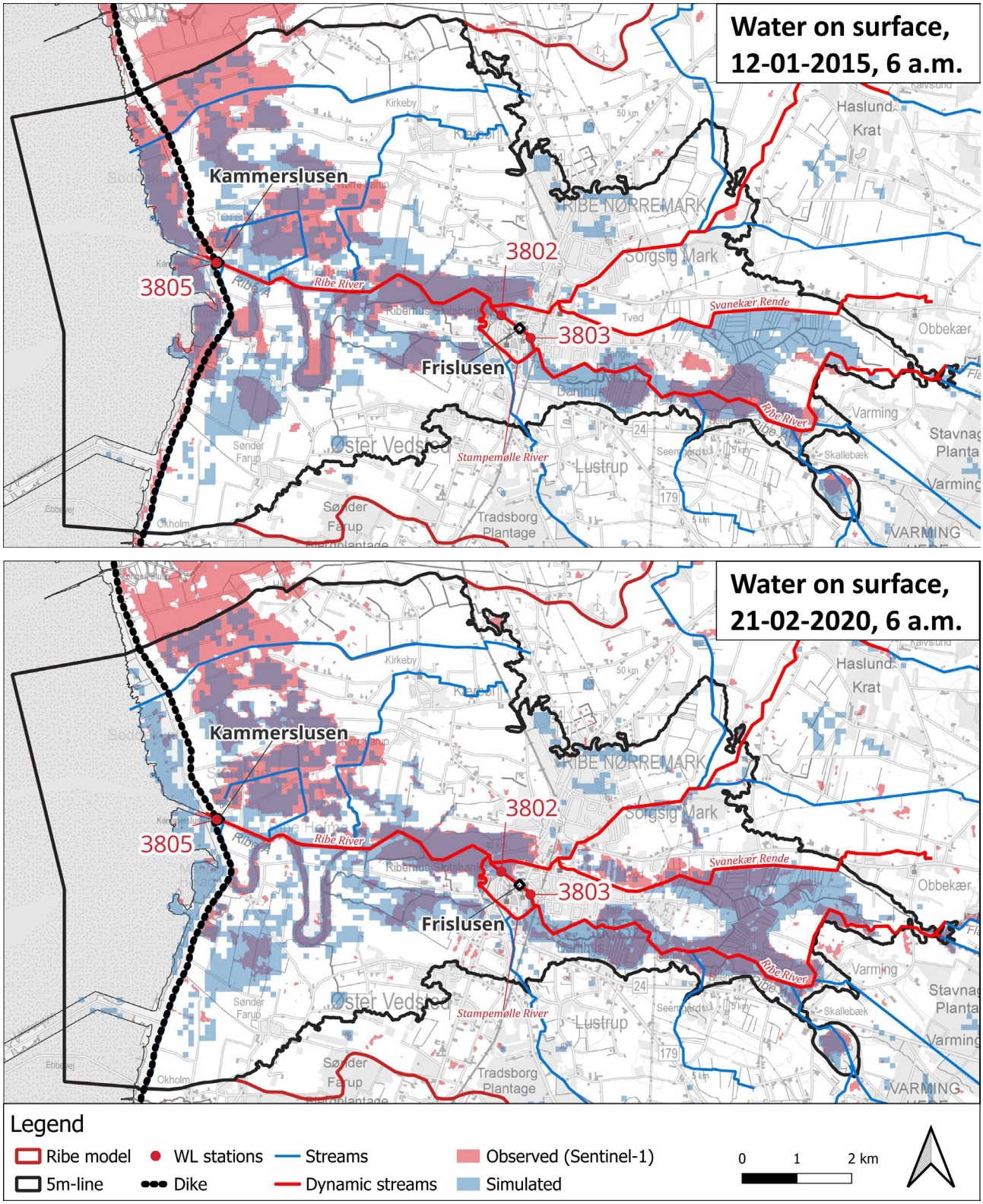

Figure 5: Spatial extent of water on surface during the flooding events of 12/01/2015 (top) and 21/02-2020 (bottom).

4.2 River stage extremes and events

The result of the entire extreme river analysis for all eight locations can be seen in Figure 6 and S-Table 4. Generally, a two-year event is 1.97 meters above sea level downstream of Ribe, while a 100-year event is 2.7 meters. Here the bank elevation around the stream lies between 1.8 and 2 meters. Upstream of the Frisluse (located between WL3802 and WL3803), the bank elevations are between 2-2.8 meters above sea level, and here a 2-year event corresponds to 2.5 meter above sea level, while a 100-year event is equivalent to3.1 meter. The model shows that the river sluice is generally closed 61% of the time during the 30 years. The most common is that a closing sequence lasts 6-8 hours, and the vast majority of all closing sequences are less than 10 hours (98%). The remainder of the closing sequences are majorly between 10-30 hours with a maximum sequence of 59 hours closing time.

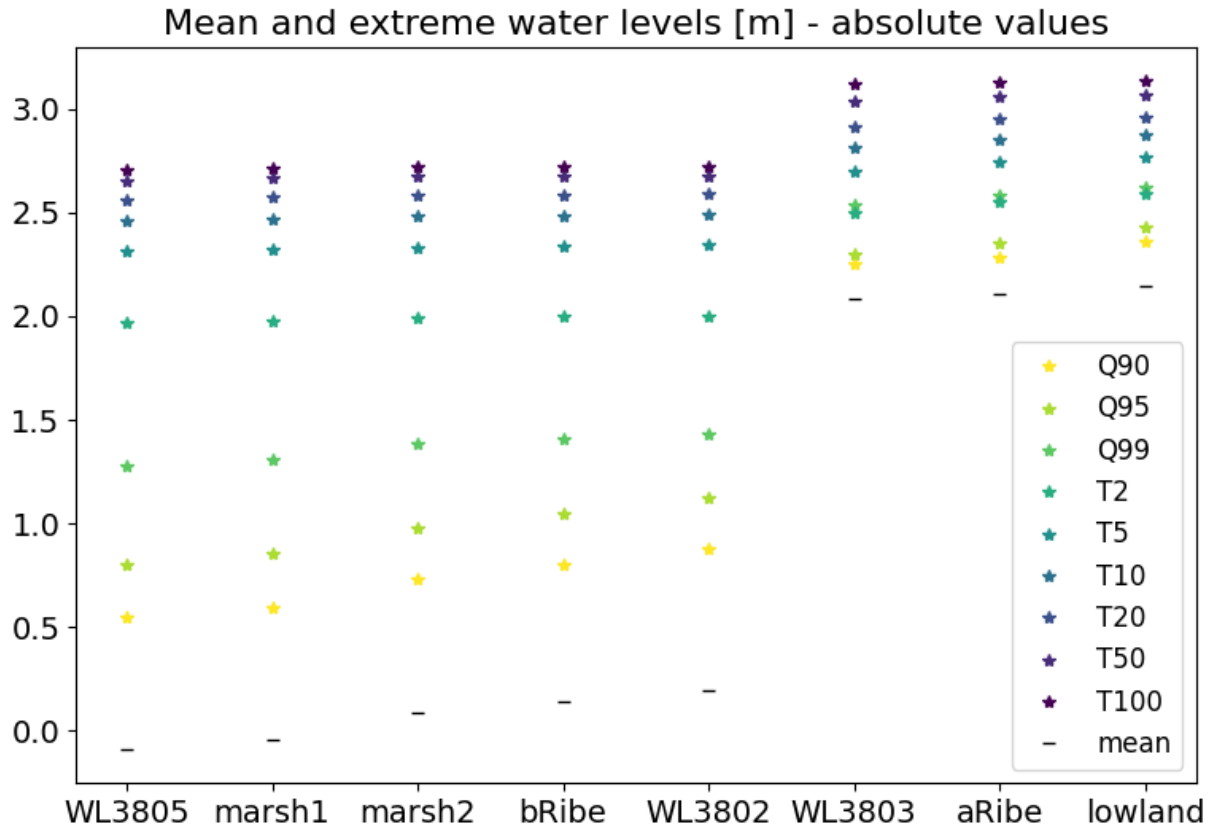

Figure 6 Resulting extreme event analysis of the river stage at selected stream locations (see Figure 1 for location).

The river water level can then be used for event identification based on the adopted identification method. The most important threshold to estimate is the threshold as this is the values above which it is assumed that flooding is likely to occur. The initial idea was to use the actual bank elevation at the eight locations as the threshold for flooding, however, this was quickly found to present a number of problems. Firstly, bank elevations are highly uncertain as cross section data are often of poor data quality and outdated. Secondly, this means that bank elevations may change substantially from one grid to the neighbouring grid. This implies that the location of where the water level is extracted becomes very important. It was therefore chosen to use the Q90 water level as the flood thresholds. Comparing the bank elevation to the Q90 water level showed that the equivalent

water stage was above bank elevation most of the time at the selected locations, and therefore the Q90 water level was assumed to be a good threshold identifier for the potential occurrence of flood.

Using the Q90, exceedances are merged in time (at each location) and space (across all river locations), giving rise to a total of 6429 river events. However, as expected, many of these events are only separated by a few hours and can thus not be counted as separate non-correlated events. Actually, 90% of events are separated by less than 24 hours. Correlation thresholds of 24, 48 and 72 hours were tested resulting in 667, 360 and 270 unique events, respectively. At the end, the correlation threshold was specified to 24 hr, so that events are merged when they are separated by less than 24 hours. Out of the 667 unique events, 413 are only occurring at one or two locations on the river, with a maximum size of Q90. It was therefore chosen to set the minimum number of location with exceedance to two locations, thus omitting these small local events from the analyses; resulting in a total of 254 unique river stage events. An overview of the resulting events is provided in Figure 7, with the maximum extreme duration and maximum peak timing illustrated. It is clear that the majority of river events are less severe Q90, Q95, and Q99 events, and that the bulk of the events occur during winter and fall. Only few events are present during summer, and these are often low severity and short duration.

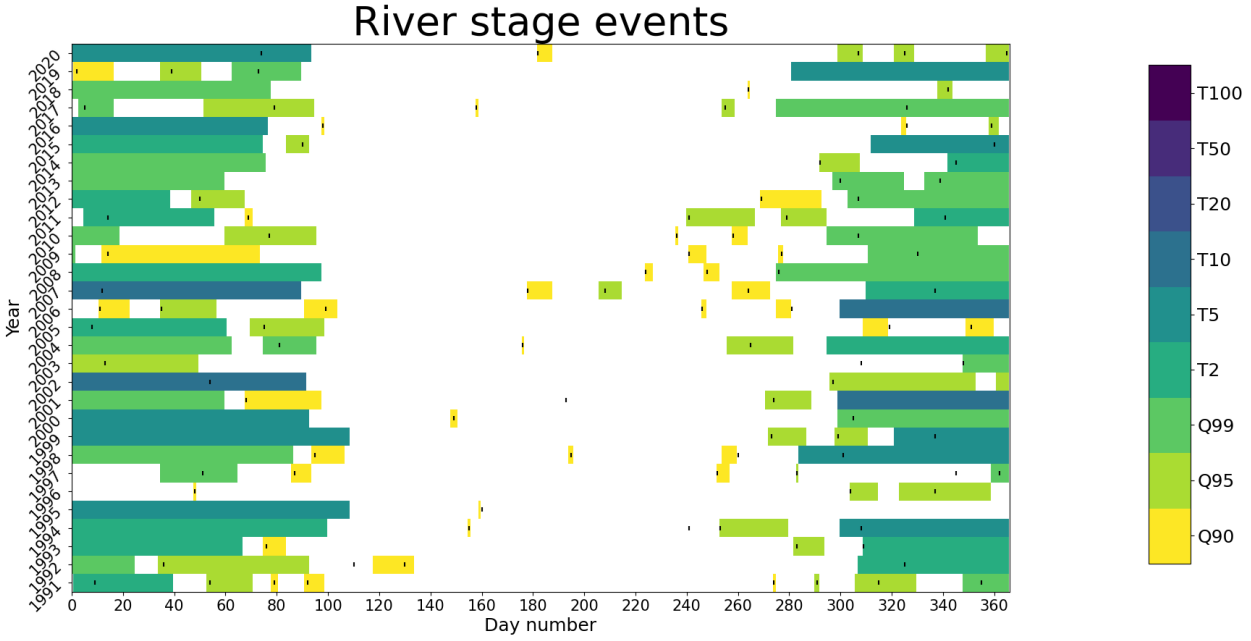

Figure 7 Overview of unique river stage events, the black lines on the chart indicate timing of max peak extreme.

In the 30-year time series there are 18 major events. Two of the 18 have T10 peaks, six events with T5 peaks, and 10 are T2-events. The characteristics of these large events are shown in Table 3, the largest T10 events are at the top and the smaller T2 at the bottom, within each group the events are sorted according to largest water level exceedance.

512 **Table 3 Identified major river stage events**

NO	DATE			DURATION [days]	TYPE
	START	STOP	MAX		
1	10-01-2002	14-03-2002	23-02-2002	62.6	T10
2	05-11-2006	08-02-2007	12-01-2007	95.1	T10
3	26-11-1999	14-01-2000	03-12-1999	48.5	T5
4	09-12-2015	05-01-2016	26-12-2015	27.1	T5
5	08-02-2020	25-03-2020	14-03-2020	45.6	T5
6	11-10-1998	27-11-1998	28-10-1998	47.7	T5
7	31-01-1999	02-04-1999	05-02-1999	61.1	T5
8	04-12-1994	13-03-1995	01-02-1995	98.5	T5
9	22-12-2004	29-01-2005	08-01-2005	37.6	T2
10	10-12-2014	04-02-2015	11-12-2014	56.0	T2
11	08-01-1993	07-02-1993	24-01-1993	29.5	T2
12	02-12-2011	15-01-2012	07-12-2011	43.9	T2
13	26-01-2000	02-04-2000	30-01-2000	66.3	T2
14	03-12-1993	17-02-1994	28-01-1994	76.6	T2
15	05-01-2008	15-02-2008	01-02-2008	40.9	T2
16	12-01-2011	23-01-2011	14-01-2011	10.9	T2
17	28-02-1994	10-04-1994	06-03-1994	40.5	T2
18	22-01-2016	13-02-2016	29-01-2016	21.3	T2

513

514 4.3 Precipitation, sea level and groundwater extremes

515 The characteristics of the precipitation and sea level extremes are shown in Figure 8. All
516 return-period information including Q90, Q95 and Q99 can be seen in S-Table 4. As expected, the
517 count of events decreases from the low extremes to the very extreme and rare conditions. For a 2-
518 year precipitation event (T2) the threshold is 31 mm/day. For reference, the annual precipitation for
519 the period is 995 mm with a monthly mean of 83 mm/month, thus more than one third of a month
520 worth of precipitation should arrive during one day. For a return period of 100 years (T100) the values
521 are 57 mm/day, but no occurrence of this size is present in the time series. The largest occurrences
522 are two high extremes with a return period of 20 and 50 years, respectively.

523 For the sea level data, the mean sea level is 0.24 m.a.s.l., being highest in December with 0.32
524 m.a.s.l. and lowest in April with 0.16 m.a.s.l. Here a 2-year occurrence (T2) corresponds to a sea level
525 of 3.13 meters above sea level, this occurs 52 times in the time series. A T100 event is reached when
526 the sea level is above 5.16 m.a.s.l. during an hour (registered on one occasion), while there are two
527 and one T50 and T20 occurrences, respectively.

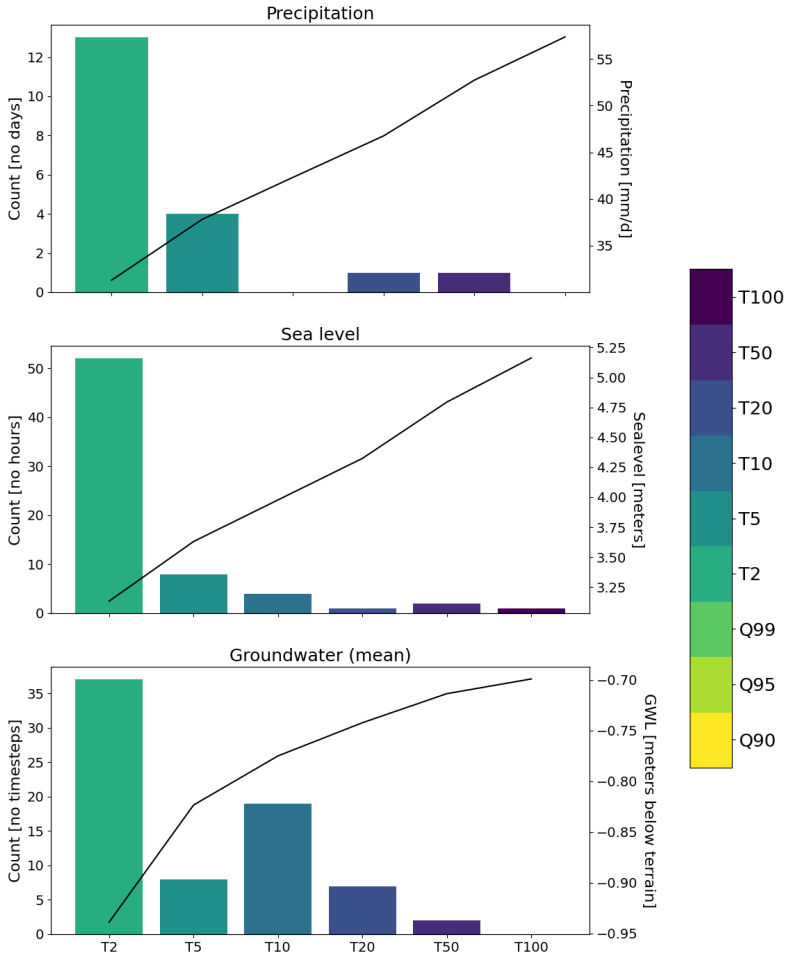

Figure 8 Count of occurrence of extremes (bars) during 1991-2020 for precipitation (top) and sea level (centre) and groundwater levels (bottom). The absolute values of the extreme thresholds are indicated by the black line (axis to the right).

The statistics for groundwater are available for every grid cell within the area of interest. An example of the resulting statistics is shown in Figure 9 where a 14-day-statistics for the phreatic groundwater level for a two-years (T2) and 100-years (T100) occurrences are shown. For many parts of the area below the 5-meter elevation line a two-year event for the groundwater is close to or above zero, meaning that the groundwater table is at ground surface. Thus, high risk of frequent groundwater flooding is estimated. The accumulated occurrence T2 and T100 events for every grid cell during the 30-year period is also shown in Figure 9.

For the mean areal groundwater level an extreme value analysis is performed (Figure 8), showing that 2-year event (T2) corresponds to a mean groundwater level of 94 cm below ground surface. For a return period of 100 years (T100) the mean groundwater level is 70 cm below surface. Two high extremes with a return period of 50 years can be seen, while seven 20 years events are registered.

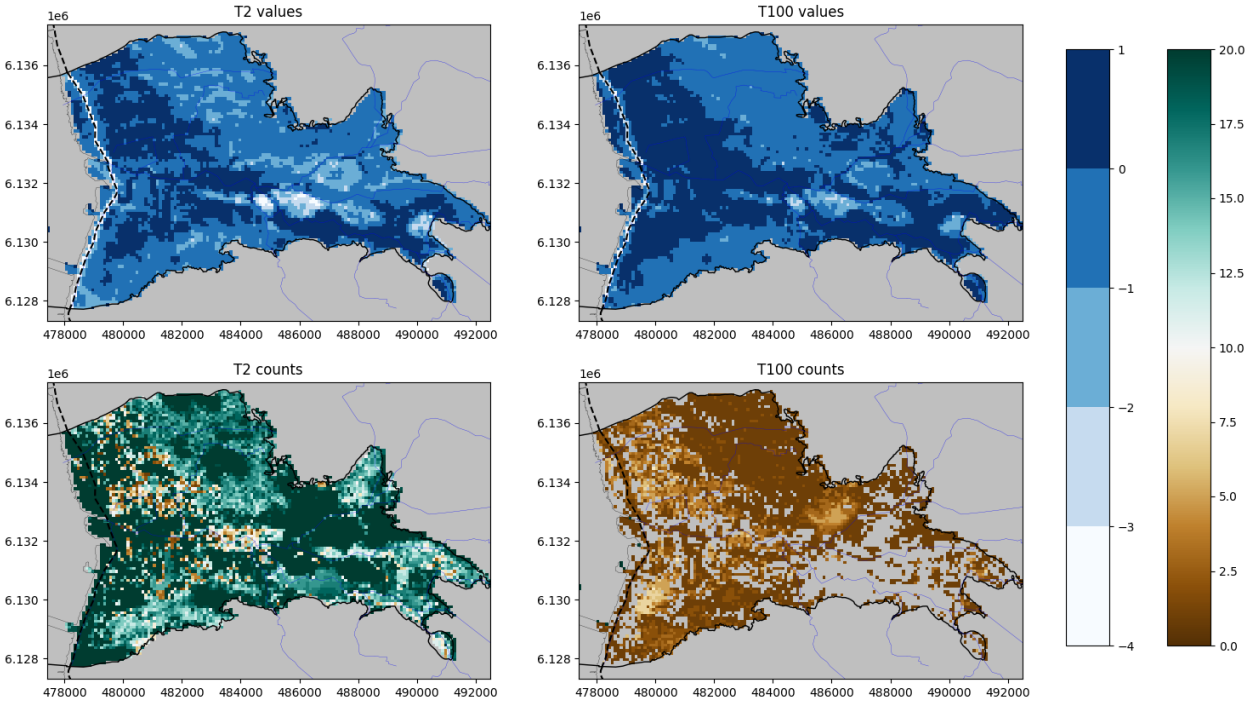

Figure 9 The top two panels show the EVA statistics of the phreatic groundwater level for a 2-years event (left) and a 100-year event (right). The bottom two panels show the accumulated count of T2 and T100 events for every grid cell during the 30 years.

4.4 Compound hazard effects

With the river stage events identified, the co-occurring events for the forcing and catchment state can be investigated. The first step is to establish the buffers to be applied when investigating the status of precipitation and sea level during the river events. For the precipitation there is higher correlation for a buffer of plus one day combined with minus 1, 2 or 4 days (S-Table 5). A simple test using the Ribe model showed that a synthetic high precipitation event registered as a maximum peak in the river stage after 1-2 days. Hence, the buffer was specified to +/- 1 day ($Pbuffer_{before}$ and $Pbuffer_{after}$= 1 day). For the sea level the correlation is generally high, but the signal is not as clear (S-Table 6). There are elevated correlations for buffers of –2.5 day after the river maximum event and at +3.5 days before combined with -5 days after. Close investigation of observed high sea level events in 1999, 2015 and 2020 where sea level influence are well-documented, showed shifts of -1 to +5 days between the highest sea level and the highest river level. In the end a buffer window of +/-5 days was adopted ($SLbuffer_{before}$ and $SLbuffer_{after}$= 5 day).

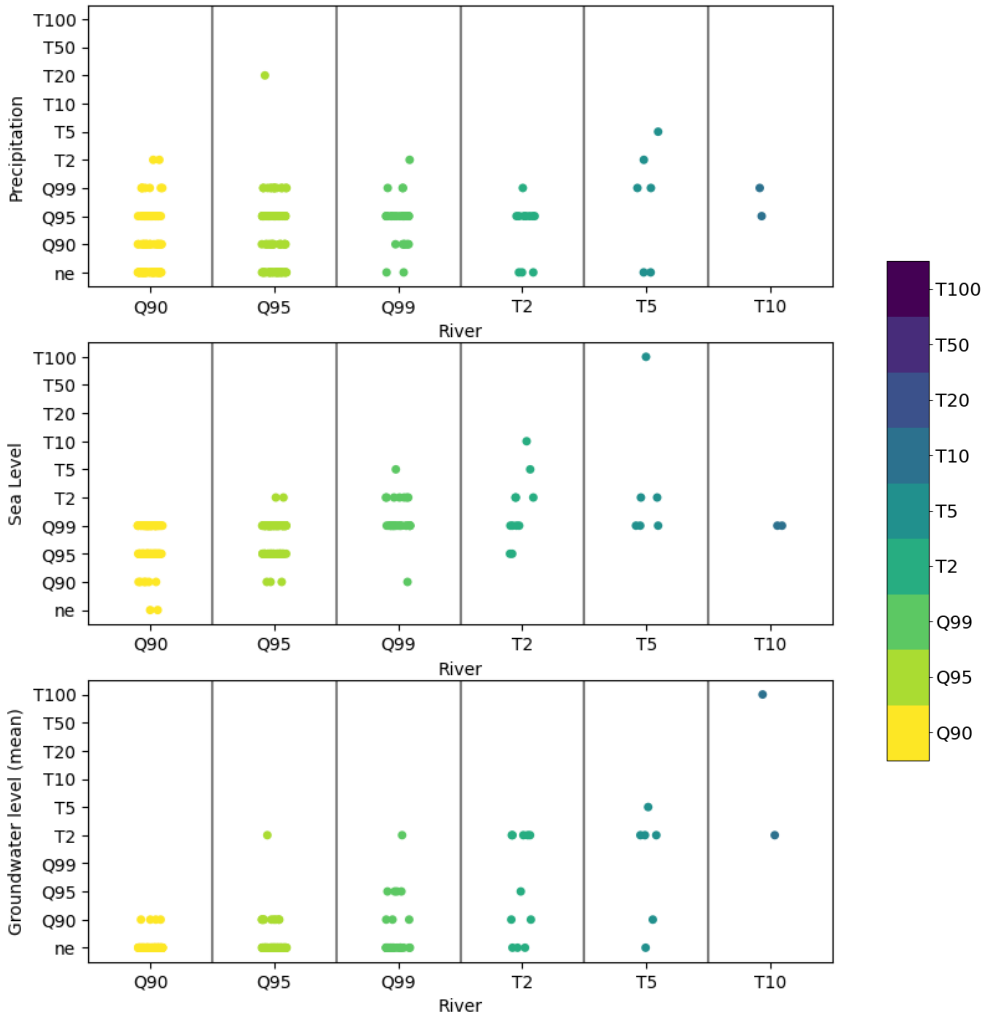

Figure 10 River water level extremes in relation to extremes in the three forcing factors precipitation, sea level and shallow groundwater.

The results of the sea level, groundwater level, and precipitation extreme for all the registered water level events can be seen in Figure 10. For sea level there is an immediate tendency to a correlation between river event size and forcing event size, thus the points move towards to upper right side as river event increase in intensity. This tendency is also seen for both the precipitation and the groundwater plot, with some exceptions. However, it is also clear that a specific forcing occurrence does not always lead to the same river event extreme. It is therefore necessary to investigate the co-occurrence of the forcing and preconditioning. To investigate this, the most extreme river events are plotted showing the correlation between all four variables in Figure 11.

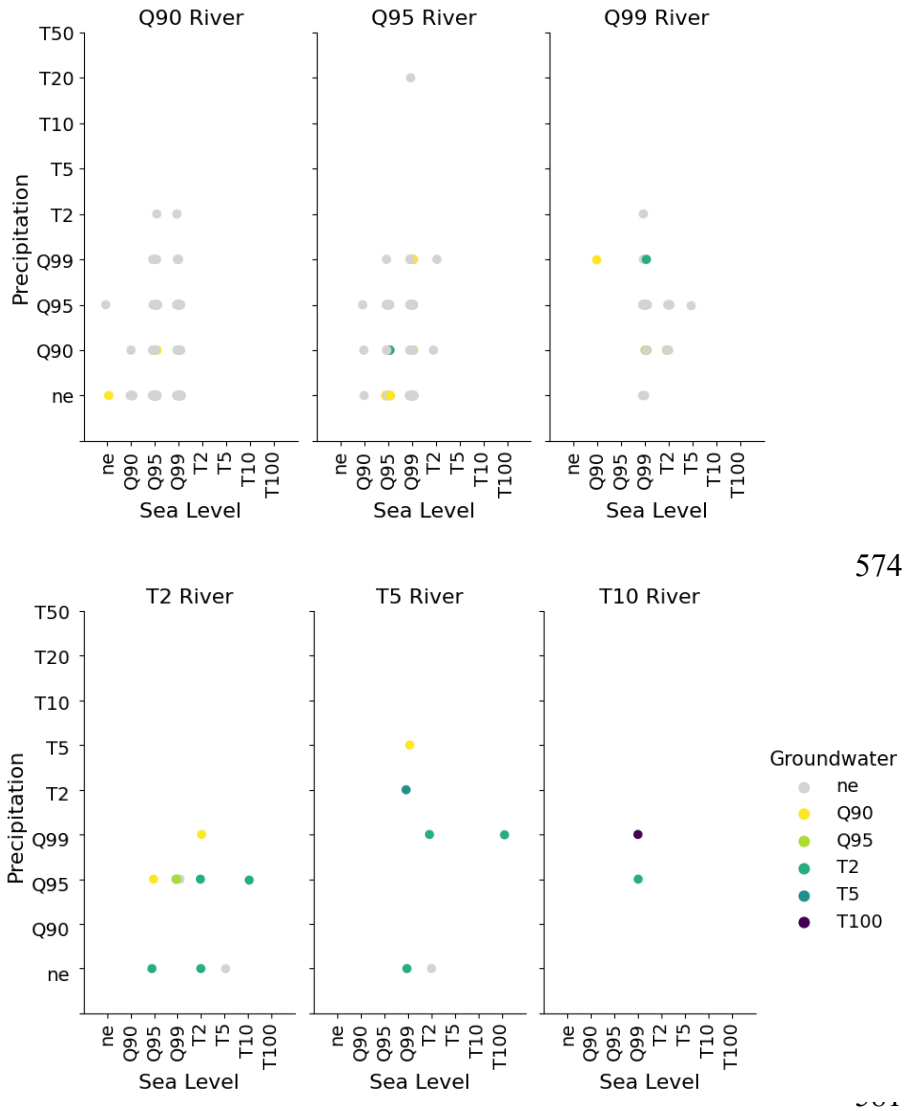

Figure 11 Combination of extremes and river event sizes. Markings registered as ne (no event) are river events where no co-occurring precipitation/groundwater/sea level extreme is registered.

The analysis shows that there is only one instance of a groundwater state (Q90) and one instance of a precipitation event potentially driving a river event without events in the other variables (ne on both y- and x-axis), both resulting in a Q90 river event. For sea level, there are 79 instances where the sea level event is present without a precipitation and groundwater extreme (resulting in river event between Q90 and T5). This highlights the strong dependence between especially river stage and sea level. There are also multiple Q90-Q99 river events where precipitation and sea level events are combined without a groundwater event.

For the 18 most extreme river events (>Q99), however, Table 4 shows that there are no extreme river events without a sea-level event above at least Q95, and of these, only two river events (no. 7 and 9) without either a precipitation or groundwater event. Thus, the same combination of sea level and precipitation can result in a smaller river event, but combined with a groundwater event, the resulting river event is generally much larger. All these variables are thus clearly important governing factors for the most extreme conditions.

Interestingly, our analysis also shows that the forcing and preconditioning of the system does not necessarily need to be very extreme to create an extreme river event response, e.g., events no. 16 and 18 have forcing and state between Q90-Q99 (annual occurring events), but in combination, they can produce a two-year maximum response in the river system. There are no compound events where T2 or higher occur in combination for all variables, thus the most extreme, and less likely, compounds are not represented in these time series.

Table 4 Identified major river stage events with corresponding forcing and preconditioning. Colors under LONGTERM indicate the highest percentile for the long-term extremes, yellow=Q90; light green=Q95; dark green>Q99, the text indicates for which rolling mean (RM) interval the largest percentile is found. No cooccurring extremes is marked with ne.

NO	RIVER EVENT TYPE	FORCING		PRECON-DITIONING				COMPOUND TYPE	LONGTERM	
		SL	P	GW	GW> Q90	GW> T2	MULTI-VAR.	PRE-COND.	SL	P
1	T10	Q99	Q95	T2	94%	79%	x	x	28RM	28RM
2	T10	Q99	Q99	T100	93%	91%	x	x	14RM	14RM
3	T5	T100	Q99	T2	85%	57%	x	x	7RM	7RM
4	T5	Q99	T5	Q90	64%	12%	x	x	7RM	7RM
5	T5	Q99	ne	T2	81%	45%		x	28RM	28RM
6	T5	T2	Q99	T2	80%	66%	x	x	7RM	14RM
7	T5	T2	ne	ne	15%	8%			21RM	28RM
8	T5	Q99	T2	T5	91%	65%	x	x	14RM	14RM
9	T2	T5	ne	ne	8%	6%			7RM	21RM
10	T2	Q99	Q95	T2	77%	59%	x	x	7RM	7RM
11	T2	T2	Q99	Q90	72%	30%	x	x	7RM	21RM
12	T2	Q99	Q95	ne	15%	6%	x		14RM	7RM
13	T2	T2	Q95	T2	91%	34%	x	x	7RM	7RM
14	T2	T2	ne	T2	93%	70%		x	7RM	7RM
15	T2	Q99	Q95	ne	7%	6%	x		7RM	28RM
16	T2	Q95	Q95	Q90	47%	23%	x	x	nodata	7RM
17	T2	Q95	ne	T2	92%	65%		x	7RM	7RM
18	T2	Q99	Q95	Q95	91%	27%	x	x	7RM	7RM

Following the classification from Zscheischler et al. (2020), the natural hazard compound events can be considered multivariate (both related to extreme sea level and precipitation) and/or preconditioned (groundwater). From Table 4 it is clear that the extreme river events are completely dominated by occurrences of compound events that are both multivariate and preconditioned (61%), while 28% are either or; and only two events (11%) are neither. For the remaining river events (Q99 and below) these numbers are 6% for both, while 58% are multivariate; and 3% are preconditioned; the remaining 33% are neither (data can be seen in S-Table 7). This is especially due to the percentage of preconditioned compound events drop for the smaller river events from 74% of all >=T2 river event (out of 18 events) being preconditioned to 9% of >=Q99 river event (out of 234 events) being preconditioned, while the multivariate are more or less constant (64% and 68%, respectively).

As mentioned, the extreme river stages may also be driven by long-term high sea levels or precipitation and not only single events. The highest percentile of the corresponding rolling means for the 18 largest river events can be seen in Table 4. 7RM indicates that the largest percentile found for the rolling mean interval are for a 7-day rolling mean window. The results show that most river events are influenced by higher-than-normal long-term sea levels and some also by long-term precipitation effects. Especially the largest river events are often correlated to long-term high precipitation. The effect of these long-term extremes versus the single events are not easy to quantify. However, there is one example (events no. 1 and 10) where the same precipitation, sea level and groundwater combination yield different river stage event (no. 1 is a T10 and no. 10 is a T2 river event). The events have more or less the same duration with respect to the river events (i.e. 56-63 days). An investigation of the long-term extremes shows that event no. 1 has a much higher long-term sea level, and that for both sea level and precipitation the higher-than-normal situation has lasted a longer period; 28 days versus 7 days. Thus, the 28-days leading up to event no. 1 has been unusual (>Q97) for both precipitation and sea level. Looking at the actual registered precipitation amount, 168 mm fell during the 28 days (corresponding to 2 months' worth of precipitation), while 90 mm fell during the 28 days for event no. 10. For sea level the average elevation above sea level for 28 days are 0.9 meter and 0.16 m for event no. 1 and 10, respectively. This is also reflected in a much higher fraction of the catchment with a groundwater level above T2 events, 79% for event no. 1 and 59% for event no. 10. This comparison thus demonstrates the high importance of looking at prolonged events in combination with single-event analysis for compound investigations.

4.5 Simulation of flooding events

The 18 highest river events are simulated by the Ribe Flood model with overbank spilling to quantify the resulting water on terrain (overland water) from these extremes. The maximum flooding timestep for each of the event can be seen in Figure 12. Generally, water on terrain is predominantly present on the outside of the sluice, around the river in the marsh, and in the old river section, as well as the lowland area to the southwest. The overall statistical results of the flood simulations can be seen in S-Table 8. The 18 largest river events generally result in flooding extent of 8-43% of the area with mean overland water depths between 0.14 to 0.35 meters, and maximum depth of 1.2 to 2.1 meters. The maximum depth may be uncertain as it can be a result of a single cell values, while the mean depth may be difficult to interpret as it is based on different numbers of cells, where the depth of water may be very small in some grids. Therefore, it was chosen to focus on the flooding extent when analysing the events. The closing time sequences of the river sluice at the sea last on average 21 hours for the 18 events.

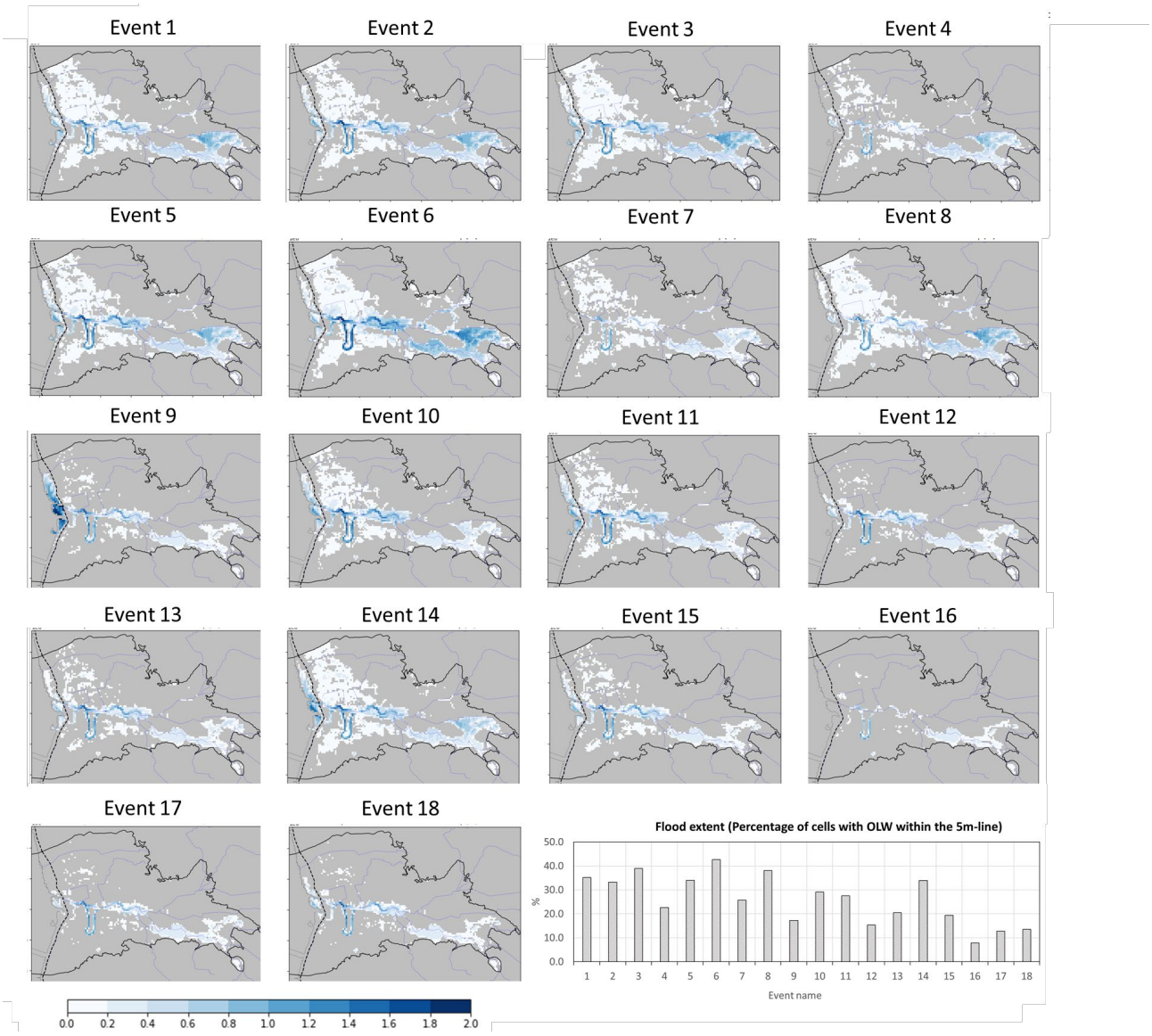

Figure 12: Maximum overland flooding from the Ribe Flood model for the 18 largest river events identified from the Ribe model. The dotted black line shows the location of the dike.

What is immediately clear is that there is not a one-to-one correlation between the river stage event analysis using the Ribe model (no flooding), and the resulting flooding when including overbank spilling (Figure 12). As an example, the largest flood extent is event no. 6 (in October/November 1998), is a T5 event. It is not the largest river event or the longest (Table 3) nor is it correlated to the largest precondition or forcing events (Table 4). This may be explained by the complicated nature of the flooding progradation, location, and timing, and highlights that analysis of river water level alone is not enough to draw conclusions, but rather that actual flood modelling (overbank spilling) in necessary to interpret system response. The fact that this river event is correlated to long-term extremes for both sea level and precipitation shows the importance of the duration of the forcing extremes.

Even though the top largest river extremes do not translate directly to the largest flood extent, there are some common traits among the flooding event with large extents. Thus, when investigating the eight largest events regarding flood extent (1,2,3,5,6,8,10,14), it can be seen that they are all

667 preconditioned events and a mean of 67% of groundwater cells above T2 (Table 4, all eight are
668 >45%), and a (mean) groundwater event of minimum T2. In comparison, the remaining flood events
669 (4,7,9,11,12,13,15,16,17,18), have a mean of 22% of groundwater cells above T2. This is also evident
670 in event 4 and 9, that are a T5 and T2 river event, but they both result small flooding extent potentially
671 related to small groundwater preconditioning. Event 17, seem to defeat these statistics, as the flood
672 extent is the second smallest of all 18 events, while the groundwater mean event is T2 with 65% of
673 cells being above T2. However, for this event the sea level event is very small (Q95), and short (no
674 long-term unordinary sea level), and no precipitation event, so little water built-up was likely present,
675 and thus limited flooding extent is registered.

676 The location of where the flooding occur is logically also correlated to the type of extreme
677 event, presumably driving the flooding situation. As an example, event 9, and event 17, is plotted
678 together in Figure 13 both events are T2 river events. Event 9 is predominantly correlated to high sea
679 level (T5), and thus the river sluice closes causing the built- up of water, as the catchment can no
680 longer drain to the ocean. The sluice was closed 32 hours during maximum sea level. This leads to
681 low-lying areas being flooding with freshwater on the inside of the dike in the marsh. However, the
682 largest flooding depths is seen on the land outside the dikes with salt water, where water depth on
683 terrain reach up to 2 meters, due to the rising sea level. For event 17, the river event is co-occurring
684 with a much smaller sea level event (Q95), where the sluice was closed for 10 hours, and a large
685 groundwater event (T2). For this event the water on terrain is predominantly flooded with freshwater
686 from within the catchment.

687 The Ribe Flood model is run in two versions for each river event: a version that allows
688 overbank spilling from the river that typically results in water on terrain. This is a result of fluvial
689 flooding combined with groundwater flooding (Figure 12). The second version, without overbank
690 spilling, flooding is a result of groundwater flooding alone (S-Figure 4). The difference between these
691 two simulations thus indicates the contribution of groundwater to the resulting flooding of the land
692 area. However, it is only an indication, as in reality the groundwater levels are affected by the river
693 stage (Abboud et al., 2018). As a very simple test, multiplying the number of flooded cells, their area,
694 and average overland water depth indicates the amount of flood water during the event (S-Table 8).
695 Estimating this amount for runs with and without overbank spilling can then be used to calculate the
696 fraction of water *may* originate from groundwater. This simple approach indicates that the
697 groundwater contribution is between 28% and 85% of the water during the events with a mean of
698 42%. It was also found that the larger flood water amounts the smaller the groundwater contribution
699 (relatively). In the example from before with event 9 and 17, the two events also have very different
700 groundwater contributions as event 9 has 28% and event 17 has 51% of flood water coming from
701 groundwater, reflecting the potential dominating source of the flooding (river built-up in event 9 and
702 high groundwater in event 17). For other event this correlation is not as clear (e.g., event 7 where
703 groundwater contribution is very high, but no groundwater extreme is present), pointing to that this
704 calculation of groundwater flood water quantities is highly uncertain. In regards of the extent, the
705 resulting flood extent was almost the same for the runs with and without the overbank spilling,
706 however the depth of the water on terrain much smaller. Thus, the areas flooded are essentially the
707 same, but much less water on terrain is present.

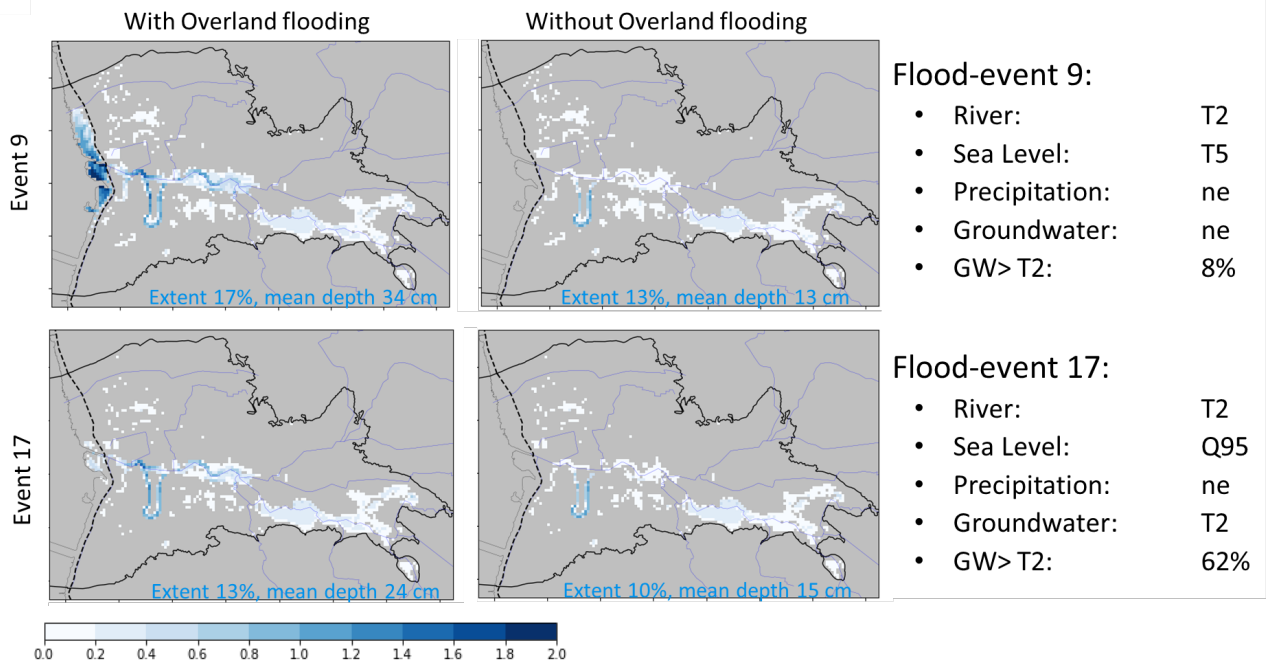

Figure 13: Overland flooding from the Ribe Flood model for event 9 (top) and event 17 (bottom). To the left is the flood simulation with overland flooding allowed from the stream, while the right image shows the resulting flood without allowing overbank spilling, thus mainly the groundwater response. The dotted black line shows the location of the dike.

5 Discussion

5.1 Hydraulic river flow and flood model

The first objective of this study was to set up and calibrate a hydraulic river flow model for the Ribe catchment capable of simulating the river locks and any tidal impacts on river water levels, the Ribe model. The adopted approach, where the structures, the boundary condition (sea level), and the improvement of the geometry of the downstream river was included, proved successful by replicating the water level from monitoring stations in the river network. An additional improvement was obtained by manual calibration of the Manning number. RMSE was reduced from 2.9m to 0.25m at the station just upstream the sluice. Calibration of the Manning number did not change the performance of the model with respect to stream discharge. Furthermore, the model showed acceptable reproduction of extreme events, including situations where the river lock is closed and water levels at the outlet increased in response of accumulation of water from the catchment that is drained by the river network. During the extreme events, build-up of water was registered in the river system as overbank spilling was not allowed in the Ribe model version.

Construction of a hydraulic river flow model, the Ribe Flood model, made it possible to simulate the water levels during extreme events with a much higher accuracy. The computational demand made it impossible to calibrate the flood model e.g., for Manning numbers, as the entire period cannot be run with overbank spilling. Thus, the Ribe Flood Model must rely on parameters found for the Ribe Model. However, the match to the measured data is found to be acceptable, both in situations where average conditions and extreme situations are considered.

735 The performance of the Ribe Flood model was validated against flooding events and
736 compared to satellite flood information. The validation of the flooding events proved difficult as
737 satellite images where often not available at the time of maximum flooding, partly due to the limited
738 acquisition time frequency of 6 days (see section 2.1), and partly because of the uncertainties
739 associated with the translation of satellite images into water on terrain. The evaluation, however,
740 suggested that the Ribe Flood model was able to replicate the flooded areas in most instances. There
741 is, however, a need for more data to validate flooding events like this, especially ground truth data as
742 e.g., drone images (Iqbal et al., 2023), citizen science e.g, photos (Peña et al., 2022) and piezometers
743 (Neri-Flores et al., 2019). Additionally, future modelling efforts assessing flooding may seek to
744 include the impact of cascading events like dam breaks or sediment deposits in drainage systems,
745 though it would require information on location and timing of such events, which may not be readily
746 available. These limitations are especially important if models like this are used in climate adaptation
747 plans and risk assessment plans. In this case scenarios could be developed where dam breaks and/or
748 sedimentation deposits are considered.

749 5.2 Using the river stage for event analysis and flood proxy

750 The extreme events for the river stages were investigated using the EVA tool on multiple sites
751 on the river. The idea behind investigating several locations on the river, was to identify occurrences
752 of unusual river stage events with a certain propagation in the system. However, this approach also
753 led to some technical difficulties as events may be delayed and overlaying both in time and space. In
754 this study an event identification scheme was therefore adopted, merging events in time and space,
755 and subsequently filtering small events out using different thresholds. The implication of using this
756 method is not easy to quantify, especially timing of the beginning, end and maximum of each event
757 is subject to substantial uncertainty. Of these three dates the timing of the river peak is the most
758 important as it is used for the compound event analyse. The peak timing is estimated as the date-time
759 where the highest percentile exceedance on the river is reached. This timing may not be precisely the
760 same for every river point, thus making this value ambiguous. However, it is assumed that the river
761 stages are highly correlated and the maximum peak in one location may not be substantially different
762 from the maximum peak in another. A buffer period was therefore introduced when looking for co-
763 occurring extremes in precipitation, sea level and groundwater. The choice of this buffer period was
764 based on a Spearman Rank correlation targeting the highest correlation values, but the final choice of
765 buffer period still adds to the uncertainty.

766 Another approach would have been to choose a single point on the river for the river event
767 analysis. However, the choice of a representative river point is also subjective. It can be speculated
768 that the uncertainty is probably larger for the smallest events, as the choices of thresholds and merging
769 methods are more likely to mask smaller river stage exceedances, while the largest events are
770 routinely preserved across procedures. However, to confirm this, more research is necessary.

771 The flood analysis from the result of the Ribe Flood Model showed that the extent of the flood
772 was not directly predictable from the river extreme analysis from the Ribe model, as the largest return
773 period events did not result in the largest flooding extent and depth. This is not completely surprising
774 as flooding extents are also related to duration and location of the river extreme.

775 5.3 Compound analysis

776 In this study we have tried to use a bottom-up approach by focusing on the resulting extremes
777 in river and overland flooding, and from them investigating the forcing that may have led to these

results, as the reverse approach suggested by Zscheischler et al, (2018). It is however important to state that a co-occurrence is not statistical evidence for a driver causing the flooding. But based on system knowledge and natural response in the hydrological system a co-occurring driver extreme is assumed to be the driving force of the flooding response. Furthermore, the resulting extremes that have been investigated for their contributing variables, are not necessarily equal to actual impacts (anthropogenic and natural disasters) registered in the catchment, again highlighting the need for ground truth data during floods.

From the analysis in this study it was shown that no unique indication of a specific compound event combination (strength) is required to generate high river/flooding conditions. But rather that several different combinations of the drivers could give rise to the same high river stage, but that the resulting location of the actual flooding on terrain would to some degree differ depending on governing drivers. However, the river events are greatly dominated by co-occurring sea level events, and for the largest events the vast majority also have other compounding drivers. Thus, highlighting the importance of including multiple compounding sources in flood investigations (Bates et al., 2021; Pasquier et al., 2019).

Furthermore, from the 18 largest river stage events, both the high river stages and the flooding simulation seem to indicate a relationship between the largest flooding events and the preconditioning (shallow groundwater state). As the largest high river stage events as well as the flooding events with the largest flood extent all have high shallow groundwater preconditioning states. The compounding effect from shallow and deep groundwater have not received much attention in literature. Rahimi et al. (2020) used an analytical tool to investigate the impact of groundwater, precipitation, and sea level for the San Leandro watershed in Oakland Flatland, USA, generating inundation maps based on these effects. A 2-year precipitation event was combined with high tide, 1meter sea level rise and groundwater inundation, caused by sea level rise, finding that incorporating groundwater into the assessment greatly enhanced flooding extents. There is thus a great need for incorporating groundwater (preconditioning) into compound evaluating for low-lying coastal zones with high shallow groundwater tables and assessing the groundwater contribution to flooding events (Bosserelle et al., 2022).

This study is focusing on the compounding effects from terrain-near groundwater, but since deep groundwater pressure interacts with shallow groundwater levels with a different time memory, there may be correlation that are being overlooked. There may also be other drivers such as groundwater abstraction, or groundwater discharge to the sea that may potentially impact flood risks, however more research is needed here and generally more in-depth research is required on correlations between the various flooding drivers and the compound, cascading, and systemic risks they cause (Sulfikkar Ahamed et al., 2023). Apart from these potential correlations and wider risk issues not incorporated fully, the effect of duration and long-term extremes seems to be particularly important for the catchment, as long-term high precipitation and prolonged closed sluice conditions greatly accelerate the water built-up. Long-term extremes should therefore also be incorporated into the compound effect analysis. Especially areas where river structures are present to protect inland areas, the risks of closing a sluice will greatly depend on catchment state and the long-term water flux to the system.

The study investigates water on terrain and the flooding extent but has not investigated the water quality of the floodwater. The impact of flood water type, i.e. salt or fresh water could have large impacts on biodiversity, ecosystems, crop yield and farming as well as the release of greenhouse gases such as methane from the flooded areas.

The issues investigated in this study may potentially escalate in a future climate under global change conditions. A future sea level rise has the potential to heighten the impact of storm surges and may lead to longer closing time of the sluice in the future. A study by Colgan et al. (2022) showed that the Ribe area could potentially be looking into a sea level rise of 55 cm for the SSP2-4.5 AR6 and 75 cm for a SSP5-8.5AR6 at the end of the century and 85 and 123 cm by 2150. Simultaneously, there is a mean projected increase in precipitation for the Danish area in end of the century of +76mm/yr and +165 mm/yr for RCP4.5 AR5 and RCP8.5 AR5 scenarios, respectively (Pasten-Zapata et al., 2019). As the current mean annual precipitation is 857 mm/yr for Denmark, this change is substantial. Seidenfaden et al. (2022) found that this projected precipitation change lead to a mean of 12 cm groundwater increase for western Jutland, and a 16 cm increase for the highest 5th percentile (closest to terrain). The issues of flooding in this area thus may be even larger in a future climate and the problem with backwater flooding even more pressing.

6 Conclusions

In this study, we applied two versions of a detailed fully coupled hydrological model to a tidal affect catchment in Denmark. The aim was to successfully simulate the complex feedback in the hydrological system from the river sluice at the sea level, precipitation, and groundwater dynamics. From the extreme value analyses for river water stages, sea levels, precipitation, and groundwater levels this study also tried to identify compound effects on the occurrence of high river stages and overland flooding. Here, it was generally found that:

- Sea level was major controller of high river stages, however for the largest events compounding effect (both preconditioned and multivariate) were continually present.
- Especially, high groundwater state (wet preconditioning in the catchment) lead to larger flooding extents and higher river stages.
- The duration of the elevated sea level or high precipitation were also shown to be important for the flooding impact.

This analysis has also shown that the hydrological system is extremely complex and compounding effects may be overlaying, depending on strength, length, preconditioning, extent, and definitions. Thus, there is a general need to make sure to account for all governing variables when investigating and predicting the impact of compound events in low-lying coastal areas. Especially the effect of groundwater has been previously understudied, and seems, as shown in this case, to be very important. Furthermore, there is a need to develop frameworks that incorporate both the effect from single large extreme events as well as prolonged extreme events into compound analyses.

Acknowledgements

The authors wish to acknowledge the GeoCenter Denmark funding of the SeaLevelRise project of which this paper is part of. The paper would not have been possible without the support of this funding source. A special thanks to colleagues, Maria Ondracek and Raphael Schneider at the department of Hydrology, GEUS for technical assistance.

Open Research

In this study the commercial model software Mike She and Mike Hydro have been used, the model code and software are therefore not publicly assessable. The results and data used in this study however can be made available on request. Several dataset are already available for download through public platforms. The sea level data on https://www.dmi.dk/frie-data, stream data on

https://odaforalle.au.dk/ and groundwater heads on https://eng.geus.dk/products-services-facilities/data-and-maps/national-well-database-jupiter.

7 References

Abbott, M.B., Bathurst, J.C., Cunge, J.A., O'Connell, P.E., Rasmussen, J., 1986. An introduction to the European hydrological system – systeme hydrologique europeen, "She", 2: Structure of a physically-based, distributed modeling system. Journal of Hydrology, 87: 61-77.

Abboud, J.M., Ryan, M.C., Osborn, G.D., 2018. Groundwater flooding in a river-connected alluvial aquifer. Journal of Flood Risk Management, 11(4): e12334. DOI:https://doi.org/10.1111/jfr3.12334

Anselmo, V., Galeati, G., Palmieri, S., Rossi, U., Todini, E., 1996. Flood risk assessment using an integrated hydrological and hydraulic modelling approach: a case study. Journal of Hydrology, 175(1): 533-554. DOI:https://doi.org/10.1016/S0022-1694(96)80023-0

Bates, P.D. et al., 2021. Combined Modeling of US Fluvial, Pluvial, and Coastal Flood Hazard Under Current and Future Climates. Water Resources Research, 57(2): e2020WR028673. DOI:https://doi.org/10.1029/2020WR028673

Bevacqua, E. et al., 2021. Guidelines for Studying Diverse Types of Compound Weather and Climate Events. Earth's Future, 9(11): e2021EF002340. DOI:https://doi.org/10.1029/2021EF002340

Bevacqua, E. et al., 2019. Higher probability of compound flooding from precipitation and storm surge in Europe under anthropogenic climate change. Science Advances, 5(9): eaaw5531. DOI:doi:10.1126/sciadv.aaw5531

Bosserelle, A.L., Morgan, L.K., Hughes, M.W., 2022. Groundwater Rise and Associated Flooding in Coastal Settlements Due To Sea-Level Rise: A Review of Processes and Methods. Earth's Future, 10(7): e2021EF002580. DOI:https://doi.org/10.1029/2021EF002580

Colgan, W. et al., 2022. Sea-level rise in Denmark: paleo context, recent projections and policy implications. GEUS Bulletin, 49. DOI:10.34194/geusb.v49.8315

DCA, 2014. Den Danske Jordklassificering.

DHI, 2019. User Guide, DHI – Water & Environment, Hørsholm, Denmark.

DHI, 2020. MikeShe User Guide and Reference Manual, DHI – Water & Environment, Hørsholm, Denmark.

DHI, 2024. EVA - User Guide, DHI – Water & Environment, Hørsholm, Denmark.

DMI, 2022. Frie Data - https://www.dmi.dk/friedata/observationer/.

Dutta, D., 2011. An integrated tool for assessment of flood vulnerability of coastal cities to sea-level rise and potential socio-economic impacts: a case study in Bangkok, Thailand. Hydrological Sciences Journal, 56(5): 805-823. DOI:10.1080/02626667.2011.585611

900 Dykstra, S.L., Dzwonkowski, B., 2021. The Role of Intensifying Precipitation on Coastal River
901 Flooding and Compound River-Storm Surge Events, Northeast Gulf of Mexico. Water
902 Resources Research, 57(11): e2020WR029363. DOI:https://doi.org/10.1029/2020WR029363

903 ESA, 2023a. Copernicus dataspace. European Space Agency (ESA).

904 ESA, 2023b. ESA's Sentinel Application Platform Software.

905 ESA, 2023c. Sentinel-1 SAR User Guide. In: Signature, E.S.A. (Ed.), User Guides. ESA.

906 GEUS, 2014. National well database JUPITER. GEUS, Copenhagen, Denmark.

907 Heinrich, P. et al., 2023. Compound flood events: analysing the joint occurrence of extreme river
908 discharge events and storm surges in northern and central Europe. Nat. Hazards Earth Syst.
909 Sci., 23(5): 1967-1985. DOI:10.5194/nhess-23-1967-2023

910 Hendry, A. et al., 2019. Assessing the characteristics and drivers of compound flooding events around
911 the UK coast. Hydrol. Earth Syst. Sci., 23(7): 3117-3139. DOI:10.5194/hess-23-3117-2019

912 Henriksen, H.J. et al., 2020. Udvikling af landsdækkende modelberegninger af terrænnære
913 hydrologiske forhold i 100m grid ved anvendelse af DK-modellen, GEUS.

914 Henriksen, H.J. et al., 2023. A New Digital Twin for Climate Change Adaptation, Water
915 Management, and Disaster Risk Reduction (HIP Digital Twin). Water, 15(1): 25.

916 Henriksen, H.J. et al., 2003. Methodology for construction, calibration and validation of a national
917 hydrological model for Denmark. Journal of Hydrology, 280: 52-71.

918 HIP, 2022. Hydrologisk Information og Pronose System. In: SFDE (Ed.).
919 DOI:https://hip.dataforsyningen.dk/help

920 Historiskatlas, 2023. Kammerslusen. Esbjerg Kommunes Biblioteker, Sydvestjyske Museer.

921 Højberg, A.L., Troldborg, L., Stisen, S., Christensen, B.B.S., Henriksen, H.J., 2013. Stakeholder
922 driven update and improvement of a national water resources model. Environmental
923 Modelling & Software, 40(0): 202-213. DOI:http://dx.doi.org/10.1016/j.envsoft.2012.09.010

924 Iqbal, U., Riaz, M.Z.B., Zhao, J., Barthelemy, J., Perez, P., 2023. Drones for Flood Monitoring,
925 Mapping and Detection: A Bibliometric Review. Drones, 7(1): 32.

926 Kew, S.F., Selten, F.M., Lenderink, G., Hazeleger, W., 2013. The simultaneous occurrence of surge
927 and discharge extremes for the Rhine delta. Nat. Hazards Earth Syst. Sci., 13(8): 2017-2029.
928 DOI:10.5194/nhess-13-2017-2013

929 Leonard, M. et al., 2014. A compound event framework for understanding extreme impacts. WIREs
930 Climate Change, 5(1): 113-128. DOI:https://doi.org/10.1002/wcc.252

931 Levin, G., Jepsen, M.R., Blemmer, M., 2012. Basemap, Technical documentation of a model for
932 elaboration of a land-use and land-cover map for Denmark, Aarhus University, DCE,
933 http://www.dmu.dk/Pub/TR11.pdf.

934 Lian, J.J., Xu, K., Ma, C., 2013. Joint impact of rainfall and tidal level on flood risk in a coastal city
935 with a complex river network: a case study of Fuzhou City, China. Hydrol. Earth Syst. Sci.,
936 17(2): 679-689. DOI:10.5194/hess-17-679-2013

937 Magnan, A.K. et al., 2022. Sea level rise risks and societal adaptation benefits in low-lying coastal
938 areas. Scientific Reports, 12(1): 10677. DOI:10.1038/s41598-022-14303-w

939 Makkink, G.F., 1957. Examination of the Penman formula. Journal of Agricultural Science, 5: 290-
940 305.

941 McGranahan, G., Balk, D., Anderson, B., 2007. The rising tide: assessing the risks of climate change
942 and human settlements in low elevation coastal zones. Environment and Urbanization, 19(1):
943 17-37. DOI:10.1177/0956247807076960

944 Neri-Flores, I., Moreno-Casasola, P., Peralta-Peláez, L.A., Monroy, R., 2019. Groundwater and River
945 Flooding: The Importance of Wetlands in Coastal Zones. Journal of Coastal Research,
946 92(sp1): 44-54, 11.

947 Neumann, B., Vafeidis, A.T., Zimmermann, J., Nicholls, R.J., 2015. Future Coastal Population
948 Growth and Exposure to Sea-Level Rise and Coastal Flooding - A Global Assessment. PLOS
949 ONE, 10(3): e0118571. DOI:10.1371/journal.pone.0118571

950 Odaforalle, 2021. Overfladevandsdatabasen - https://odaforalle.au.dk/main.aspx.

951 Pasquier, U., He, Y., Hooton, S., Goulden, M., Hiscock, K.M., 2019. An integrated 1D–2D hydraulic
952 modelling approach to assess the sensitivity of a coastal region to compound flooding hazard
953 under climate change. Natural Hazards, 98(3): 915-937. DOI:10.1007/s11069-018-3462-1

954 Pasten-Zapata, E., Sonnenborg, T.O., Refsgaard, J.C., 2019. Climate change: Sources of uncertainty
955 in precipitation and temperature projections for Denmark. Geological Survey of Denmark and
956 Greenland Bulletin, 43: e2019430102-01-e2019430102-06.
957 DOI:https://doi.org/10.34194/GEUSB-201943-01-02

958 Peña, F. et al., 2022. Compound flood modeling framework for surface–subsurface water interactions.
959 Nat. Hazards Earth Syst. Sci., 22(3): 775-793. DOI:10.5194/nhess-22-775-2022

960 Piontkowitz, T., Madsen, H.T., Sørensen, C., 2011. Digeoversigt, Syd- og Sønderjylland.
961 Kystdirektoratet, Lemvig, pp. 132.

962 Poulter, B., Halpin, P.N., 2008. Raster modelling of coastal flooding from sea-level rise. International
963 Journal of Geographical Information Science, 22(2): 167-182.
964 DOI:10.1080/13658810701371858

965 Qiang, Y. et al., 2021. Urban flood analysis for Pearl River Delta cities using an equivalent drainage
966 method upon combined rainfall-high tide-storm surge events. Journal of Hydrology, 597:
967 126293. DOI:https://doi.org/10.1016/j.jhydrol.2021.126293

968 Rahimi, R., Tavakol-Davani, H., Graves, C., Gomez, A., Fazel Valipour, M., 2020. Compound
969 Inundation Impacts of Coastal Climate Change: Sea-Level Rise, Groundwater Rise, and
970 Coastal Precipitation. Water, 12(10): 2776.

971 Santiago-Collazo, F.L., Bilskie, M.V., Hagen, S.C., 2019. A comprehensive review of compound
972 inundation models in low-gradient coastal watersheds. Environmental Modelling & Software,
973 119: 166-181. DOI:https://doi.org/10.1016/j.envsoft.2019.06.002

974 Scharling, M., Kern-Hansen, C., 2012. Climate Grid Denmark - Dataset for use in research and
975 education, DMI, Copenhagen, Denmark.

976 Schneider, R., Henriksen, H.J., Koch, J., Troldborg, L., Stisen, S., 2021. Using machine learning to
977 downscale simulations of climate change induced changes to the shallow groundwater table,
978 EGU General Assembly 2021, Online. DOI:https://doi.org/10.5194/egusphere-egu21-7170

979 Seidenfaden, I.K., Sonnenborg, T.O., Stisen, S., Kidmose, J., 2022. Quantification of climate change
980 sensitivity of shallow and deep groundwater in Denmark. Journal of Hydrology: Regional
981 Studies, 41: 101100. DOI:https://doi.org/10.1016/j.ejrh.2022.101100

982 Seneviratne, S.I. et al., 2012. Changes in Climate Extremes and their Impacts on the Natural Physical
983 Environment. In: Field, C.B., Dahe, Q., Stocker, T.F., Barros, V. (Eds.), Managing the Risks
984 of Extreme Events and Disasters to Advance Climate Change Adaptation: Special Report of
985 the Intergovernmental Panel on Climate Change. Cambridge University Press, Cambridge,
986 pp. 109-230. DOI:DOI: 10.1017/CBO9781139177245.006

987 Sulfikkar Ahamed, M., Sarmah, T., Dabral, A., Chatterjee, R., Shaw, R., 2023. Unpacking systemic,
988 cascading, and compound risks: A case based analysis of Asia Pacific. Progress in Disaster
989 Science, 18: 100285. DOI:https://doi.org/10.1016/j.pdisas.2023.100285

990 Tang, B., Gallien, T.W., 2023. Predicting Compound Coastal Flooding in Embayment-Backed Urban
991 Catchments: Seawall and Storm Drain Implications. Journal of Marine Science and
992 Engineering, 11(7): 1454.

993 Teng, J. et al., 2017. Flood inundation modelling: A review of methods, recent advances and
994 uncertainty analysis. Environmental Modelling & Software, 90: 201-216.
995 DOI:https://doi.org/10.1016/j.envsoft.2017.01.006

996 TheDanishNatureAgency, 2023. De 5 største stormfloder i Vadehavet. Ministry of Environment of
997 Denmark, Nature Agency.

998 Wahl, T., Jain, S., Bender, J., Meyers, S.D., Luther, M.E., 2015. Increasing risk of compound flooding
999 from storm surge and rainfall for major US cities. Nature Climate Change, 5(12): 1093-1097.
1000 DOI:10.1038/nclimate2736

1001 Zellou, B., Rahali, H., 2019. Assessment of the joint impact of extreme rainfall and storm surge on
1002 the risk of flooding in a coastal area. Journal of Hydrology, 569: 647-665.
1003 DOI:https://doi.org/10.1016/j.jhydrol.2018.12.028

1004 Zscheischler, J. et al., 2020. A typology of compound weather and climate events. Nature Reviews
1005 Earth & Environment, 1(7): 333-347. DOI:10.1038/s43017-020-0060-z

1006
1007

8 Supplementary material

S-Table 1 Detailed performance for water levels 2008-2020.

		HIP4Plus MODEL			Ribe model		
Station no.	**River name and chainage**	**ME**	**MAE**	**RMSE**	**ME**	**MAE**	**RMSE**
WL3802	Ribe Aa, 11020	1.06	1.06	1.11	0.00	0.13	0.17
WL3803	Ribe Aa, 10374	0.53	0.56	0.61	-0.03	0.08	0.10
WL3805	Ribe Aa, 16874	2.98	2.98	3.00	0.07	0.18	0.23
WL3836	Stampemølleaa, 1117	-0.04	0.21	0.27	-0.12	0.20	0.25
WL3837	Hjortvadaa, 6713	0.41	0.44	0.53	0.37	0.39	0.47
WL3839	Hjortvadaa, 9055	0.41	0.50	0.61	0.23	0.27	0.35
WL3851	Hjortvadaa, 6966	0.42	0.42	0.45	0.38	0.38	0.41

S-Table 2 Detailed performance for groundwater levels 2008-2020.

		HIP4PLUS MODEL			**RIBE MODEL**		
WELL NO.	**Layer**	**ME**	**MAE**	**RMSE**	**ME**	**MAE**	**RMSE**
140.1315_1	6	1.30	1.30	1.32	1.25	1.25	1.28
140.1316_1	8	1.74	1.74	1.78	1.68	1.68	1.73
140.224_1	8	6.46	6.46	6.46	6.28	6.28	6.28
141.766_1	8	-1.25	1.25	1.25	-1.25	1.25	1.25
141.927_1	10	-6.18	6.18	6.24	-6.19	6.19	6.25
142.280_1	6	-2.31	2.31	2.34	-2.31	2.31	2.34
142.559_1	2	-2.06	2.06	2.06	-2.06	2.06	2.06
150.406_1	6	-1.34	1.34	1.34	-1.34	1.34	1.34
150.465_1	6	-0.84	0.84	0.84	-0.84	0.84	0.84
150.532_1	6	0.96	0.96	0.97	0.96	0.96	0.97
150.548_1	6	0.06	0.09	0.16	0.06	0.09	0.16
150.631_1	6	-0.93	0.93	0.94	-0.93	0.93	0.94
150.662_1	8	2.17	2.17	2.18	2.17	2.17	2.18
150.663_1	8	2.46	2.46	2.47	2.46	2.46	2.47
150.679_1	5	0.61	0.99	1.03	0.61	0.99	1.03
151.921_1	8	1.58	1.58	1.58	1.58	1.58	1.58

1013 **S-Table 3 Detailed performance for discharge stations in 2008-2020.**

	STATION NO.	RIVER NAME AND CHAINAGE	ME	MAE	RMSE	STDRES	R(CORRELATION)	R2(NASHSUTCLIFFE)
HIP4PLUS MODEL	Q380019	Jelsaa, -5400	0.02	0.04	0.08	0.08	0.92	0.82
	Q380020	Jelsaa, -6772	0.02	0.05	0.09	0.09	0.83	0.66
	Q380023	Hjortvad Aa, 2182	0.26	0.61	0.97	0.94	0.77	0.47
	Q380024	Ribe Aa, 506	-0.39	1.69	2.75	2.72	0.91	0.78
	Q380097	Gels Aa, 8116	0.04	0.36	0.53	0.52	0.87	0.58
RIBE MODEL	Q380019	Jelsaa, -5400	0.02	0.04	0.08	0.08	0.92	0.82
	Q380020	Jelsaa, -6772	0.02	0.05	0.09	0.09	0.82	0.66
	Q380023	Hjortvad Aa, 2182	0.26	0.61	0.98	0.94	0.77	0.46
	Q380024	Ribe Aa, 506	0.32	1.67	2.68	2.66	0.90	0.79
	Q380097	Gels Aa, 8116	0.04	0.36	0.53	0.52	0.87	0.58

1014

1015 **S-Table 4 Extreme analysis for sea level and precipitation. Precipitation values in parenthesis**
1016 **indicates the summed precipitation across the moving average period.**

	PRECIPITATION MM/DAY	SEA LEVEL M. A. SL.	RIVER LOCATIONS M. A. SL.							
LOC	catchment	WL3804	WL3805	marsh1	marsh2	bRibe	WL3802	WL3803	aRibe	Lowl
Q90	8.6	1.0	0.5	0.6	0.7	0.8	0.9	2.3	2.3	2.4
Q95	12.5	1.2	0.8	0.8	1.0	1.0	1.1	2.3	2.3	2.4
Q99	22.0	1.8	1.3	1.3	1.4	1.4	1.4	2.5	2.6	2.6
T2	31.3	3.1	2.0	2.0	2.0	2.0	2.0	2.5	2.6	2.6
T5	37.8	3.6	2.3	2.3	2.3	2.3	2.3	2.7	2.7	2.8
T10	42.3	4.0	2.4	2.4	2.4	2.4	2.4	2.8	2.8	2.9
T20	46.8	4.3	2.5	2.5	2.5	2.5	2.5	2.9	2.9	3.0
T50	52.7	4.8	2.6	2.6	2.6	2.6	2.6	3.0	3.0	3.1
T100	57.4	5.2	2.6	2.7	2.7	2.7	2.7	3.1	3.1	3.1

1017
1018

1019

1020 **S-Table 5 Spearman rank correlation of precipitation and river events for different buffers**

NEGATIVE BUFFER - DAYS AFTER RIVER EVENT	POSITIVE BUFFER - DAYS BEFORE RIVER EVENT									
		0	1	2	3	4	5	6	7	8
	0	0.18	0.27	0.23	0.25	0.25	0.25	0.25	0.23	0.22
	1	0.20	0.27	0.23	0.25	0.25	0.25	0.25	0.23	0.22
	2	0.20	0.23	0.23	0.25	0.25	0.25	0.25	0.23	0.22
	3	0.20	0.25	0.25	0.25	0.25	0.25	0.25	0.23	0.22
	4	0.25	0.25	0.25	0.25	0.25	0.25	0.25	0.23	0.22
	5	0.21	0.25	0.25	0.25	0.25	0.25	0.25	0.23	0.22
	6	0.20	0.25	0.25	0.25	0.25	0.25	0.25	0.23	0.22
	7	0.19	0.23	0.23	0.23	0.23	0.23	0.23	0.23	0.22
	8	0.19	0.22	0.22	0.22	0.22	0.22	0.22	0.22	0.22

1021

1022 **S-Table 6 Spearman rank correlation of sea level and river events for different buffers**

NEGATIVE BUFFER - DAYS AFTER RIVER EVENT	POSITIVE BUFFER - DAYS BEFORE RIVER EVENT																
		0	0.5	1.0	1.5	2.0	2.5	3.0	3.5	4.0	4.5	5.0	5.5	6.0	6.5	7.0	7.5	8.0
	0	0.38	0.26	0.30	0.31	0.34	0.35	0.36	0.38	0.39	0.39	0.39	0.42	0.42	0.41	0.42	0.41	0.41
	0.5	0.40	0.34	0.37	0.37	0.39	0.39	0.40	0.42	0.43	0.42	0.42	0.44	0.44	0.44	0.43	0.43	0.43
	1.0	0.47	0.38	0.41	0.41	0.42	0.42	0.43	0.45	0.46	0.46	0.46	0.46	0.47	0.46	0.46	0.46	0.46
	1.5	0.47	0.39	0.42	0.42	0.43	0.43	0.44	0.45	0.46	0.46	0.45	0.46	0.46	0.46	0.46	0.46	0.45
	2.0	0.47	0.40	0.43	0.43	0.43	0.43	0.44	0.46	0.46	0.46	0.45	0.46	0.46	0.46	0.46	0.46	0.46
	2.5	0.49	0.43	0.45	0.44	0.44	0.44	0.45	0.47	0.47	0.46	0.46	0.47	0.47	0.47	0.46	0.46	0.46
	3.0	0.49	0.43	0.45	0.45	0.45	0.45	0.46	0.47	0.48	0.47	0.47	0.47	0.47	0.47	0.47	0.46	0.46
	3.5	0.48	0.43	0.45	0.45	0.45	0.45	0.46	0.47	0.48	0.47	0.47	0.47	0.47	0.47	0.47	0.46	0.46
	4.0	0.48	0.44	0.45	0.45	0.45	0.45	0.46	0.48	0.48	0.48	0.47	0.47	0.48	0.48	0.47	0.47	0.47
	4.5	0.48	0.44	0.46	0.46	0.46	0.47	0.48	0.48	0.49	0.48	0.48	0.48	0.48	0.48	0.48	0.47	0.47
	5.0	0.48	0.45	0.47	0.47	0.47	0.47	0.48	0.49	0.49	0.49	0.48	0.49	0.49	0.49	0.49	0.49	0.48
	5.5	0.47	0.44	0.46	0.46	0.46	0.46	0.47	0.48	0.48	0.48	0.47	0.48	0.48	0.48	0.48	0.48	0.47
	6.0	0.46	0.43	0.45	0.45	0.45	0.45	0.46	0.47	0.47	0.46	0.46	0.46	0.46	0.46	0.46	0.46	0.46
	6.5	0.44	0.42	0.44	0.44	0.44	0.44	0.45	0.46	0.46	0.45	0.45	0.45	0.45	0.45	0.45	0.45	0.45
	7.0	0.44	0.42	0.44	0.44	0.44	0.44	0.45	0.46	0.46	0.45	0.45	0.45	0.45	0.45	0.45	0.45	0.45
	7.5	0.44	0.42	0.44	0.44	0.44	0.45	0.45	0.46	0.46	0.45	0.45	0.45	0.45	0.45	0.45	0.45	0.45
	8.0	0.44	0.43	0.45	0.45	0.46	0.46	0.47	0.47	0.47	0.47	0.47	0.47	0.47	0.47	0.47	0.47	0.47

1023

1024

1025 **S-Table 7 Count of multivariante and preconditioned compound events for each of the river**
1026 **event types in percentage and (count)**

RIVER EVENT	ALL	MULTIVARIATE	PRECONDITIONED	BOTH	NO COMPOUND EVENT
Q90	110	52% (57)	3% (3)	1% (1)	45% (49)
Q95	95	61% (58)	4% (4)	6% (6)	28% (27)
Q99	30	67% (20)	0% (0)	27% (8)	7% (2)
T2	11	18% (2)	18% (2)	45% (5)	18% (2)
T5	6	0% (0)	17% (1)	67% (4)	17% (1)
T10	2	0% (0)	0% (0)	100% (2)	0% (0)
T20	0	0% (0)	0% (0)	0% (0)	0% (0)
T50	0	0% (0)	0% (0)	0% (0)	0% (0)
T100	0	0% (0)	0% (0)	0% (0)	0% (0)

1027

1028

1029 **S-Table 8 Flooding statistics**

NO	DATES		TYPE	MEAN DEPTH [M]	PERCENTAGE OF CELLS WITH OL WATER [%]	MAX WATER DETPH [M]	MEAN VOLUME [M^3 WATER]	PERCENTAGE GW CONTRI-BUTION	CLOS-ING TIME [HR]
	START	STOP							
1	10-01-2002	14-03-2002	T10	0.24	35%	1.55	6.54E+06	36%	21
2	05-11-2006	08-02-2007	T10	0.26	33%	2.01	6.61E+06	33%	19
3	26-11-1999	14-01-2000	T5	0.25	39%	1.62	7.59E+06	36%	22
4	09-12-2015	05-01-2016	T5	0.21	23%	1.19	3.65E+06	47%	11
5	08-02-2020	25-03-2020	T5	0.27	34%	1.82	6.99E+06	33%	23
6	11-10-1998	27-11-1998	T5	0.35	43%	1.87	1.13E+07	28%	21
7	31-01-1999	02-04-1999	T5	0.14	26%	1.20	2.84E+06	62%	9
8	04-12-1994	13-03-1995	T5	0.22	38%	1.50	6.28E+06	47%	19
9	22-12-2004	29-01-2005	T2	0.34	17%	2.07	4.50E+06	28%	32
10	10-12-2014	04-02-2015	T2	0.24	29%	1.68	5.36E+06	35%	33
11	08-01-1993	07-02-1993	T2	0.24	28%	1.62	5.04E+06	33%	20
12	02-12-2011	15-01-2012	T2	0.27	15%	1.57	3.21E+06	38%	25
13	26-01-2000	02-04-2000	T2	0.23	20%	1.53	3.57E+06	40%	34
14	03-12-1993	17-02-1994	T2	0.25	34%	1.69	6.45E+06	35%	10
15	05-01-2008	15-02-2008	T2	0.22	19%	1.74	3.25E+06	42%	34
16	12-01-2011	23-01-2011	T2	0.19	8%	1.34	1.13E+06	85%	22
17	28-02-1994	10-04-1994	T2	0.24	13%	1.55	2.33E+06	51%	10
18	22-01-2016	13-02-2016	T2	0.25	14%	1.61	2.60E+06	42%	24

1030

1031

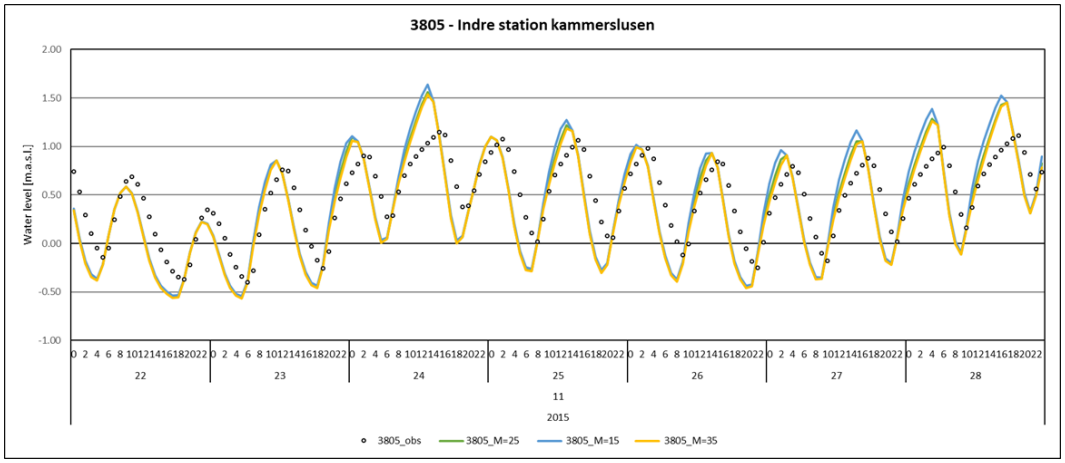

S-Figure 1: Calibration of the Manning number

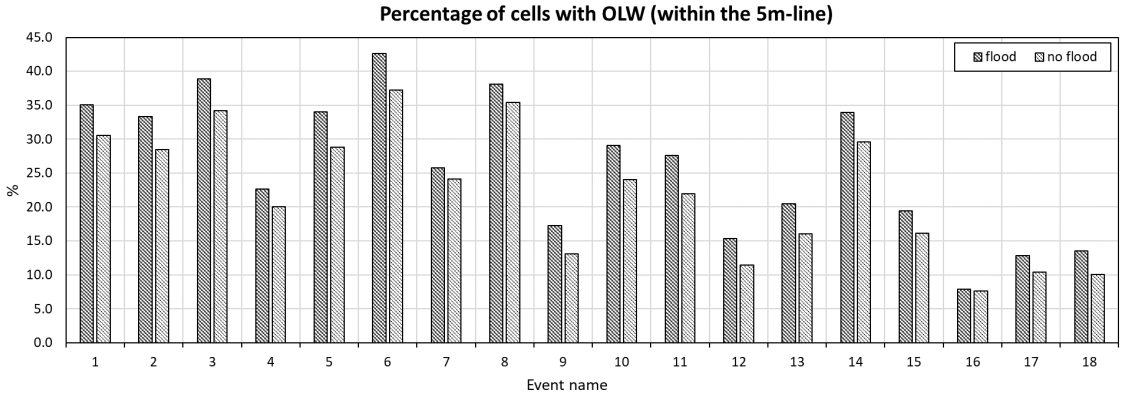

S-Figure 2: Percentage of overland water on terrain (flooding) for the area within the 5 meter line, with overbank spilling (flood) and without overbank spilling (no flood)

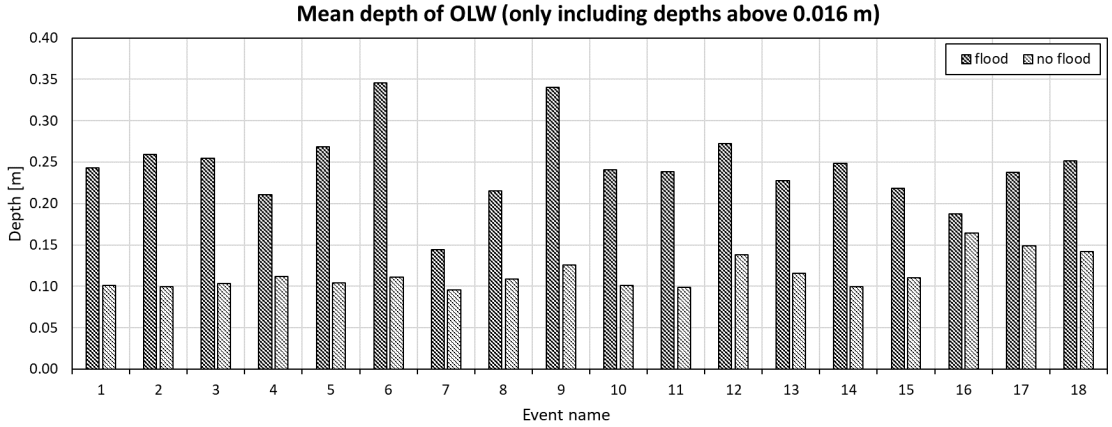

S-Figure 3: Mean depth of overland water on terrain (flooding), with overbank spilling (flood) and without overbank spilling (no flood)

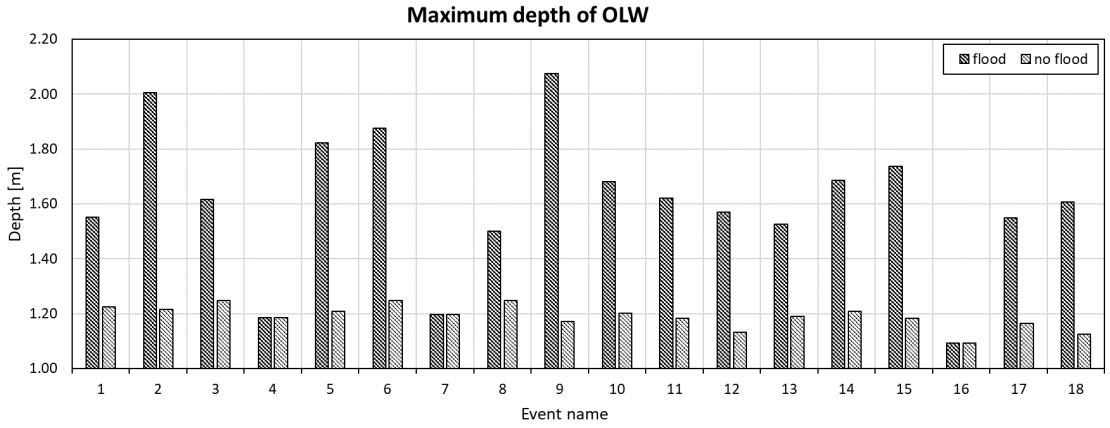

S-Figure 4: Maximum depth of overland water on terrain (flooding), with overbank spilling (flood) and without overbank spilling (no flood)

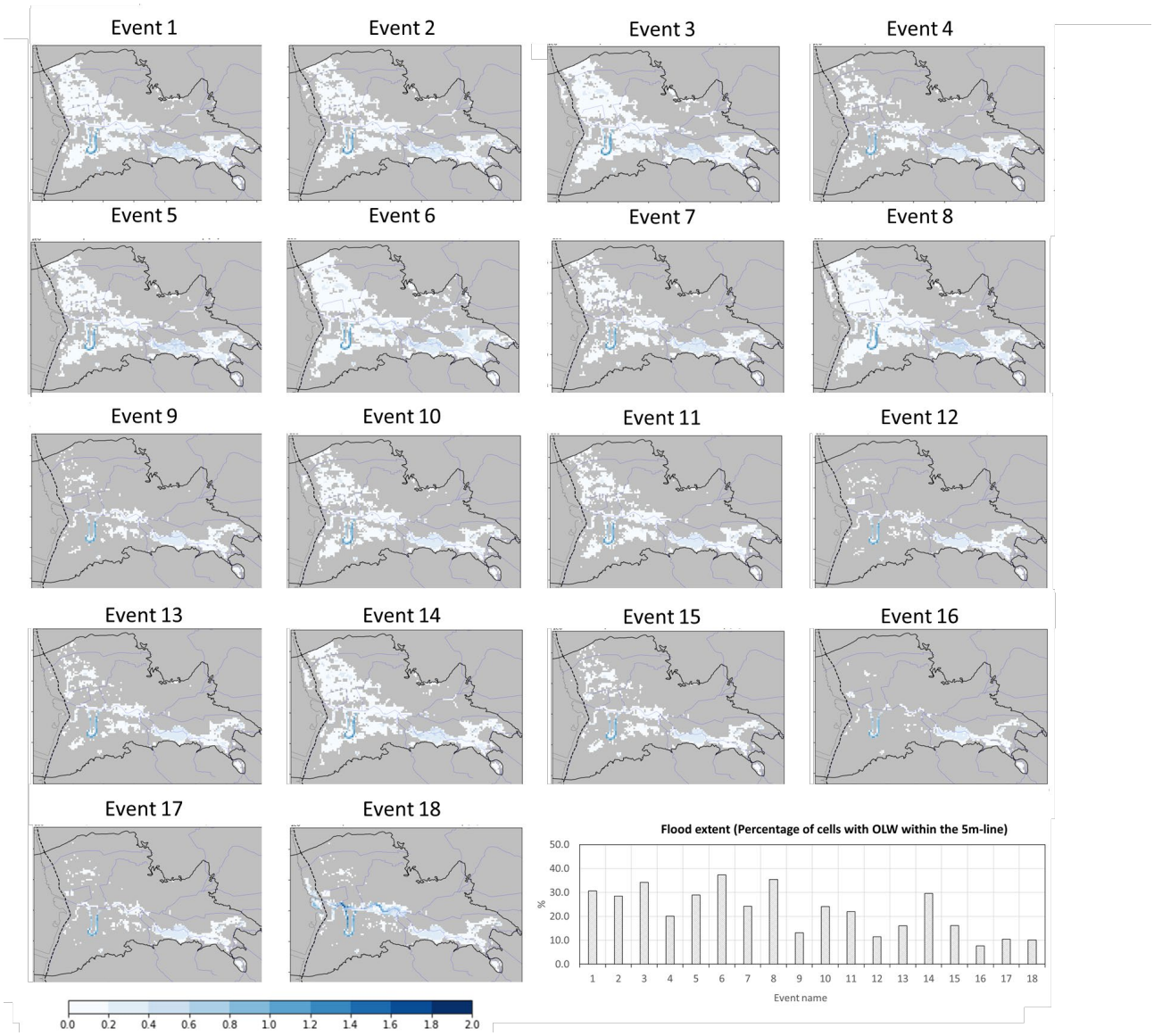

S-Figure 5: Maximum overland flooding from the Ribe Flood model for the 18 largest river events identified from the Ribe model without allowing overbank spilling in the flood model. The dotted black line shows the location of the dike.